การลดสิ่งแปลกปลอมจากโลหะในภาพเอกซเรย์คอมพิวเตอร์บริเวณศีรษะและลำคอ

นายสรจรส อุณห์ศิริ

วิทยานิพนธ์นี้เป็นส่วนหนึ่งของการศึกษาตามหลักสูตรปริญญาวิทยาศาสตรดุษฎีบัณฑิต
สาขาวิชาวิศวกรรมชีวเวช (สหสาขาวิชา)
คณะวิศวกรรมศาสตร์ จุฬาลงกรณ์มหาวิทยาลัย
ปีการศึกษา 2560

Metal artifact reduction in computed tomography at head and neck region

Mr. Sornjarod Oonsiri

A Dissertation Submitted in Partial Fulfillment of the Requirements
for the Degree of Doctor of Philosophy Program in Biomedical Engineering
Faculty of Engineering
Chulalongkorn University
Academic Year 2017

Thesis Title	Metal artifact reduction in computed tomography at head and neck region
By	Mr. Sornjarod Oonsiri
Field of Study	Biomedical Engineering
Thesis Advisor	Associate Professor Anchali Krisanachinda, Ph.D.
Thesis Co-Advisor	Assistant Professor Pizzanu Kanongchaiyos, Ph.D.
	Assistant Professor Supatana Auethavekiat, Ph.D.

Accepted by the Faculty of Engineering, Chulalongkorn University in Partial Fulfillment of the Requirements for the Doctoral Degree

....Dean of the Faculty of Engineering

(Associate Professor Supot Teachavorasinskun, D.Eng.)

THESIS COMMITTEE

....Chairman

(Associate Professor Mana Sriyudthsak, D.Eng.)

....Thesis Advisor

(Associate Professor Anchali Krisanachinda, Ph.D.)

....Thesis Co-Advisor

(Assistant Professor Pizzanu Kanongchaiyos, Ph.D.)

....Thesis Co-Advisor

(Assistant Professor Supatana Auethavekiat, Ph.D.)

....Examiner

(Associate Professor Chawalit Lertbutsayanukul, M.D.)

....Examiner

(Pakpum Somboon, Ph.D.)

....External Examiner

(Theerachai Chaitusaney, M.D.)

สรจรส อุณห์ศิริ : การลดสิ่งแปลกปลอมจากโลหะในภาพเอกซเรย์คอมพิวเตอร์บริเวณศีรษะและลำคอ (Metal artifact reduction in computed tomography at head and neck region) อ.ที่ปรึกษาวิทยานิพนธ์หลัก: รศ. ดร. อัญชลี กฤษณจินดา, อ.ที่ปรึกษาวิทยานิพนธ์ร่วม: ผศ. ดร. พิษณุ คนองชัยยศ , ผศ. ดร. สุพัฒนา เอื้อทวีเกียรติ, หน้า.

สิ่งแปลกปลอมในภาพเอกซเรย์คอมพิวเตอร์ที่เรียกว่า Streak ส่วนใหญ่เกิดจากการมีโลหะในอวัยวะภายในของผู้ป่วยที่ได้รับการถ่ายภาพด้วยเอกซเรย์คอมพิวเตอร์ ทำให้ความสามารถในการวินิจฉัยภาพลดลงหรือการวินิจฉัยผิดพลาดได้ วัตถุประสงค์ของการศึกษานี้ เพื่อพัฒนาโปรแกรมลดสิ่งแปลกปลอมที่เกิดจากโลหะในภาพเอกซเรย์คอมพิวเตอร์ โดยใช้โปรแกรม MATLAB และนำไปทดสอบในหุ่นจำลองและบริเวณศีรษะและลำคอของผู้ป่วยที่มีสิ่งแปลกปลอมในภาพเอกซเรย์คอมพิวเตอร์

โปรแกรมใหม่ที่ใช้ลดสิ่งแปลกปลอมในภาพเอกซเรย์คอมพิวเตอร์ ที่เกิดจากการมีโลหะในอวัยวะภายในของผู้ป่วยได้พัฒนามาจากโปรแกรม MATLAB ซึ่งใช้หลักการของ Non-linear interpolation ในการปรับปรุงภาพให้ดีขึ้น มีการศึกษาในหุ่นจำลองที่เป็นวัสดุเนื้อเดียวและหุ่นจำลองที่เสมือนมนุษย์ รวมทั้งในผู้ป่วยที่มีสิ่งแปลกปลอมที่เกิดจากโลหะในภาพเอกซเรย์คอมพิวเตอร์ ที่ถ่ายภาพจากเครื่องเอกซเรย์คอมพิวเตอร์ผลิตภัณฑ์ฟิลิปส์ รุ่น Brilliance Big Bore เครื่องเอกซเรย์คอมพิวเตอร์รุ่นนี้มีโปรแกรมที่ช่วยลดสิ่งแปลกปลอมในภาพเอกซเรย์คอมพิวเตอร์ที่เกิดจากโลหะ (OMAR) การวิเคราะห์ผลการใช้โปรแกรม ๓ โปรแกรมในเชิงปริมาณของภาพเอกซเรย์คอมพิวเตอร์คิดเป็นร้อยละของค่าความแปรปรวน และการวิเคราะห์ในเชิงคุณภาพของภาพเอกซเรย์คอมพิวเตอร์ได้จากการให้คะแนนโดยแพทย์รังสีรักษาและมะเร็งวิทยา 2 คน

จากผลการศึกษาพบว่า ในหุ่นจำลองที่เป็นวัสดุเนื้อเดียวและหุ่นจำลองที่เสมือนมนุษย์บริเวณศีรษะและลำคอ พบว่าโปรแกรมใหม่ที่ใช้ลดสิ่งแปลกปลอม มีประสิทธิภาพสูงกว่าโปรแกรม OMAR ผลิตภัณฑ์ฟิลิปส์ ในทางตรงข้าม โปรแกรม OMAR มีประสิทธิภาพสูงกว่าโปรแกรมใหม่ที่ใช้ลดสิ่งแปลกปลอมในผู้ป่วยบริเวณศีรษะและลำคอ สำหรับโปรแกรมใหม่สามารถลดสิ่งแปลกปลอมในภาพเอกซเรย์คอมพิวเตอร์ที่เกิดจากโลหะได้ประมาณ 40% ในหุ่นจำลองที่เป็นวัสดุเนื้อเดียว, 40% ในหุ่นจำลองที่เสมือนมนุษย์ และ 60% ในผู้ป่วยตามลำดับ การวิเคราะห์ในเชิงคุณภาพของภาพเอกซเรย์คอมพิวเตอร์จากแพทย์รังสีรักษาและมะเร็งวิทยา 2 คน ได้คะแนนเฉลี่ยใกล้เคียงกันทั้งสองโปรแกรม

ประสิทธิภาพของโปรแกรมใหม่ที่ใช้ลดสิ่งแปลกปลอมในการศึกษานี้สูงกว่าการสร้างภาพโดยวิธี Filter back projection และการใช้โปรแกรม OMAR ในหุ่นจำลองแบบเนื้อเดียวและหุ่นจำลองที่เสมือนมนุษย์บริเวณศีรษะและลำคอในช่วงค่ากระแส-เวลา, mAs ที่ใช้ทางการแพทย์ อย่างไรก็ตามประสิทธิภาพของการลดสิ่งปลอมปนโลหะสำหรับ OMAR สูงกว่าโปรแกรมใหม่ที่ใช้ลดสิ่งแปลกปลอมในการศึกษานี้และ Filter back projection การวิเคราะห์ในเชิงคุณภาพของภาพเอกซเรย์คอมพิวเตอร์จากแพทย์รังสีรักษาและมะเร็งวิทยา 2 คน ได้คะแนนเฉลี่ยใกล้เคียงกันทั้งสองวิธี

สาขาวิชา วิศวกรรมชีวเวช (สหสาขาวิชา)	ลายมือชื่อนิสิต ....
ปีการศึกษา 2560	ลายมือชื่อ อ.ที่ปรึกษาหลัก ....
	ลายมือชื่อ อ.ที่ปรึกษาร่วม ....
	ลายมือชื่อ อ.ที่ปรึกษาร่วม ....

5671429221 : MAJOR BIOMEDICAL ENGINEERING
KEYWORDS: COMPUTED TOMOGRAPHY / METAL ARTIFACT REDUCTION ALGORITHM / IMAGE QUALITY / HEAD AND NECK

SORNJAROD OONSIRI: Metal artifact reduction in computed tomography at head and neck region. ADVISOR: ASSOC. PROF. ANCHALI KRISANACHINDA, Ph.D., CO-ADVISOR: ASST. PROF. PIZZANU KANONGCHAIYOS, Ph.D., ASST. PROF. SUPATANA AUETHAVEKIAT, Ph.D., pp.

The common streak artifacts in computed tomographic images result from the metal implant in patients. Such the artifacts could suppress proper diagnosis or misdiagnosis in computed tomographic images. The purpose of this study is to develop the method for metal artifact reduction using MATLAB software and implement in both phantom and patients for head and neck computed tomographic imaging.

The new algorithm of metal artifact reduction in computed tomographic images had been developed using MATLAB software. The homogeneous phantom, Alderson Rando phantom, and patients with a metal implant in the head and neck region had been scanned by Philips Brilliance Big Bore CT. Commercial Orthopedic metal artifact reduction (OMAR) and new algorithms were applied to the computed tomographic images in phantoms and patients with the metal artifact in the head and neck region. The quantitative analysis of image quality on a metal artifact of the head and neck region was evaluated in percent noise. The qualitative analysis in clinical imaging was evaluated in scoring by two radiation oncologists.

In homogeneous and Alderson Rando phantoms, the new algorithm indicated higher efficiency in metal artifact reduction than OMAR. In contrast, for the head and neck computed tomographic image with metal artifact reduction, OMAR showed higher efficiency than the new algorithm. The new algorithm suppressed the artifact in homogeneous, anthropomorphic phantom and patients with a metal implant in the head and neck region approximate 40%, 40%, and 60%, respectively. The new algorithm of metal artifact reduction based on non-linear interpolation technique to suppress the metal artifact in computed tomographic images, use the unique technique to improve the image quality. The qualitative analysis by two radiation oncologists showed the comparable results of OMAR and new algorithm.

The efficiency of the new algorithm is better than filtered back projection and metal artifact reduction for OMAR in homogeneous phantom and Alderson Rando phantom in the clinical range of the tube current-time, mAs. However, the efficiency of metal artifact reduction for OMAR is higher than a new algorithm and filtered back projection regarding percent noise. The image quality scoring by two independent radiation oncologists with the same experience showed comparable efficiency result of the new algorithm and OMAR.

Field of Study: Biomedical Engineering
Academic Year: 2017

Student's Signature ....
Advisor's Signature ....
Co-Advisor's Signature ....
Co-Advisor's Signature ....

ACKNOWLEDGEMENTS

I would like to express gratitude and most profound appreciation to Associate Professor Anchali Krisanachinda, Ph.D., my advisor for her guidance, invaluable advice, supervision, constructive comments and English language proof in this research. I am equally grateful to Assistant Professor Pizzanu Kanongchaiyos, Ph.D. and Assistant Professor Supatana Auethavekiat, Ph.D. my co-advisors for their help in the development of new algorithm in MATLAB and kind suggestion.

I would like to sincerely thank my thesis committee, for their kindness in examining the research methodology and provide a suggestion for the improvement.

I am grateful to all lecturers and staff in Biomedical Engineering Program, Faculty of Engineering, Chulalongkorn University for their kind support and supply the knowledge in Biomedical Engineering.

I would like to thank Division of Radiation Oncology, Department of Radiology, King Chulalongkorn Memorial Hospital for financial support. This research was granted by IAEA Doctoral Coordinated Research Projected (CRP) on “Advance in Medical Imaging Techniques” (E2.40.19), I am pleased to acknowledge with thanks.

Finally, I am grateful to my family for valuable encouragement, entirely care and understanding during the entire course of study.

CONTENTS

Page

LIST OF FIGURES

LIST OF TABLES

LIST OF ABBREVIATIONS

cm	Centimeter
cm^3	Cubic centimeter
CT	Computed tomography
CTDI	Computed tomography dose index
DICOM	Digital Imaging in COmmunications in Medicine
FBP	Filtered back projection
g	Gram
GB	Gigabyte
HU	Hounsfield unit
ICRU	International Commission on Radiation Units and Measurement
IMRT	Intensity-modulated radiation therapy
IRB	Institutional Review Board
kVp	Kilovoltage peak
LDPE	Low-density polyethylene
mAs	Milliamperage-second
MB	Megabyte
MV	Megavoltage
OMAR	Metal artifact reduction for orthopedic implant
PA	Postero-Anterior
PET	Positron emission tomography
PMMA	Polymethyl methacrylate
VMAT	volumetric modulated arc therapy

Chapter 1

Introduction

Computed tomography imaging had been introduced into clinical practice since the early 1970s (1). The x-ray imaging was revolutionized, providing high image quality which the transverse axial cross-sections of the human body had been reproduced. Healthy tissues are therefore not superimposed on the image as in conventional x-ray imaging. Computed tomography is one of the most important modality for diagnostic imaging because it provides the cross-sectional images of the whole body. The clinical potential of computed tomography became apparent during its early clinical use, and the excitement forever solidified the role of computers in medical imaging. Recent advances in acquisition geometry, detector technology, multiple detector arrays and x-ray tube design have led to scanning times now measured in fractions of a second (2-7).

Modern computers deliver the power that allows reconstruction of the image data necessary in the real time. Over the past two decades, rapid speed computational system and hardware development of x-ray computed tomography technologies have been accompanied by equally advances in image reconstruction algorithms. The algorithm development can be classified into three major areas: analytical reconstruction, model-based iterative reconstruction, and application-specific reconstruction. The filtered back projection was the method for computed tomography image reconstruction based on an analytical inversion of Radon transformation. Filtered back projection is excellent and fast reconstructions in ideal conditions, but in the clinical condition, the image artifacts could be produced. This is the drawback of conventional filtered back projection. It might produce the streak artifacts in the metallic region of the computed tomographic images. The streak artifact degrades enormously the computed tomographic image quality which the radiologists could not be able to give a reliable diagnosis because the anatomies are overlapped or distorted by the artifacts (8-11).

The common artifact in computed tomographic images results from the patient's metal implant caused by multiple mechanisms, some of which are related to the metal itself, and some of which are related to the reconstruction algorithm. The metal implant can cause beam hardening and scattered effect. Metal artifact suppresses or obstructs in diagnosis or misdiagnoses as it occurred in ten percent of the patients' tomographic images (12).

Metal artifact reduction for orthopedic implant (OMAR) is the first commercial product available which implements a robust algorithm to mitigate artifacts caused by metal implants in computed tomographic images. The crux of the OMAR implementation is an iterative loop where the output correction image is subtracted from the original input image. The resultant image can then become the new input image, and the process can be repeated (13).

OMAR can induce some minor artifacts when the metal is close to air or low-density tissue. Spine with metal screws can be problematic when using metal artifact reduction for the orthopedic implant. Similarly, pacemakers can create a problem for metal artifact reduction in an orthopedic implant. Its proximity to the lung with metal wires entering the heart and lung area can cause metal artifact reduction for the orthopedic implant to induce streaking artifacts that are not present in the non-corrected image.

Another limitation of OMAR is that it does not use the DICOM file format when processing the corrected images. Therefore, it is not possible to use computed tomographic images from other vendors. This is the reason for the new algorithm development in this study uses the DICOM file format for computed tomographic images from every vendor.

This study aims to develop the method for metal artifact reduction in computed tomography imaging using MATLAB software.

Chapter 2
Theory and literature review

2.1 Basic principles of computed tomography (1)

Radon transform describes the relationship between an object and its projected image. It can be applied to reconstruct the object if there are a sufficient number of the projected images. Since its mathematical properties are beyond the scope of this thesis, the filtered back projection is used to explain the basic idea of the tomography imaging.

The intensity in x-ray imaging is the result of the attenuation along the line between the x-ray source and the detector. The information along the line is combined and lost. In case of an organ with a simple shape, the lost information can be recovered by addition projection images. As shown in figure 1, the posteroanterior (PA) image provides the information along the width and the height, while the lateral image provides the information along the height and the depth. The combination of PA and lateral images provides the 3D dimension of objects identifiable in both images, such as pulmonary nodule. However, more projection images are required to construct the complete 3D object, especially for more complex or subtle pathology. In computed tomography (CT) imaging, the projection images are taken at a uniform angular interval around a body. Each projection image provides a cross-sectional image of the body and is combined to form a 3D object by applying CT reconstruction methods such as filtered back projection.

A point in an image conveys only 2D information. However, in CT imaging, the angular distance between each slice is small leading to small slice thickness. Thus, a 2D pixel in the image can be approximated as the projection of a small uniform volume and becomes a 3D voxel (volume element). The resolution of a voxel in the projection plane is the resolution of an image, while the resolution of the remaining axis is the slice thickness.

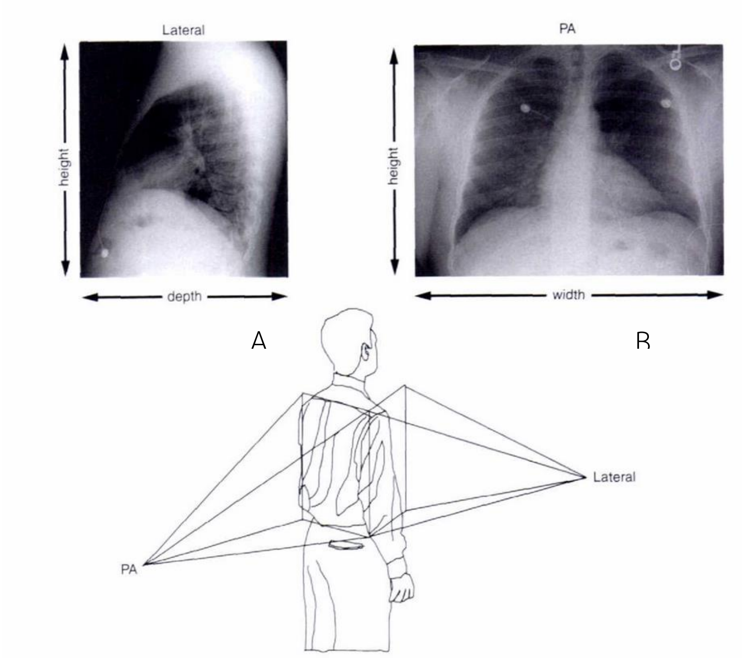

Figure 1 A: Lateral and B: Postero-Anterior (PA) chest radiographs provide three-dimensional information

The tomographic image is a picture of a slab of the patient’s anatomy. The two-dimensional computed tomography image corresponds to a three-dimensional section of the patient, so that even the computed tomography, three-dimensional objects are displayed into a two-dimensional image. However, unlike the case with plain film imaging, the computed tomography slice-thickness is very thin and is approximately uniform. The two-dimensional array of pixels in the computed tomographic image corresponding to an equal number of three- dimensional voxel in the patient. Voxels (volume elements) have the same in-plane dimensions as pixels (picture elements), but they also include the slice thickness dimension. Each pixel on the computed tomographic image displays the average x-ray attenuation properties of the tissue in the corresponding voxel.

2.2 Tomographic reconstruction (1)

In CT imaging, an x-ray travels from its source passes through a body to the detector. Its intensity is being attenuated (absorbed) in a body, and the intensity at the detector is given by the following equation.

$$I_t = I_0 e^{-(\mu_1 t_1 + \mu_2 t_2 + \cdots + \mu_n t_n)}, \qquad \text{...1}$$

where I_0 and I_t are the x-ray intensities at the source and detector, respectively. μ_i and $\mathrm{t_i}$ are a linear attenuation coefficient of an ith tissue/organ and its thickness respectively.

To simplify the reconstruction problem, the attenuation coefficient is averaged over the entire body; hence equation 1 becomes

$$I_t = I_0 e^{-\mu t}, \qquad \text{...2}$$

I_0 is an unattenuated intensity and can be measured by a reference detector; however, it is a machine-dependent value. The machine dependence can be removed by normalizing the detected intensity, I_t, by I_0. In medical imaging, we are interested in the anatomic characteristic inside a body, which can be inferred from the attenuation coefficient, μ. Instead of working on the power of an exponential, it is easier to work on the summation. So the logarithmic value is used and the parameter to be used in the reconstruction is as follows.

$$\ln(I_0/I_t) = \mu t, \qquad \text{...3}$$

where $\ln(\cdot)$ is the natural logarithm. The thickness, t, is assumed constant for every projection; hence, can be ignored.

The parameter in equation 3 has two desirable properties: (1) the independence of the CT machine and (2) dependent only on the anatomic characteristic. It is unaffected by underexposure and overexposure. In contrast, in standard x-ray imaging, the underexposure and overexposure lead to too white and too dark images, respectively.

The CT reconstruction algorithm is used to produce a 3D object from the attenuation coefficient. Filtered back projection is the most widely used algorithm in CT imaging, thanks to its low computational cost. The coefficient is smeared along the x-ray path and combined to form the 3D object. The ramp filter is applied to reduce the blurring. Iterative reconstruction has higher noise tolerant than filtered back projection. In the past, its high computing cost limited its use to the small data such as single photon emission computed tomography (SPECT). The recent advancement in algorithm design and better computer hardware lead to the feasibility of applying the iterative reconstruction for CT imaging. However, it is currently an optional feature

2.3 Filter back projection

The intensity in a projected image is the integration of attenuation coefficients along the x-ray beam and can be represented by forwarding Radon transform. In discrete domain, the integration becomes the summation, and the intensity in the projected image is merely the summation of attenuation coefficients along the line as shown in figure 2. The object's body and air are depicted as shaded and white boxes, respectively. The reconstruction problem is to construct the object when only the projected images (depicted in red, green and blue) are available. In case of a 3×3 object (as in this figure), it is possible to form nine linear equations and solve for the exact value. However, when the dimension is more massive (such as 512×512 in conventional CT slice), the computation cost for reconstructing the specific object is too high.

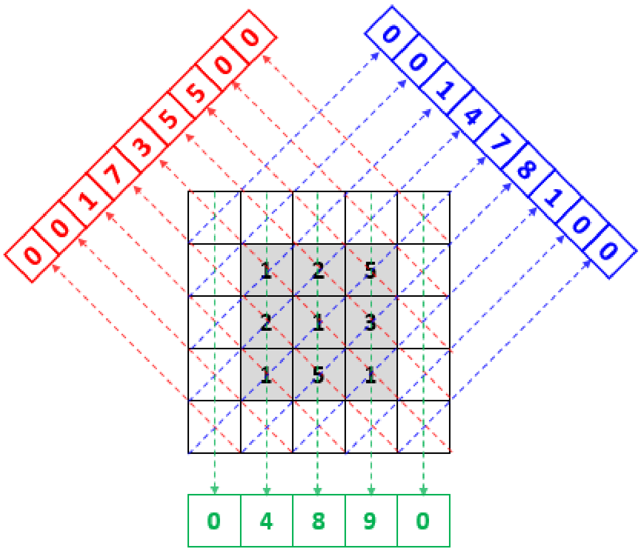

Figure 2 Parallel beam projections of an image. The object is shown as a shaded box, and the number shows the attenuation coefficient. The projected images are shown in red, green and blue.

The anatomy can be conveyed from the relative attenuation; it is unnecessary to reconstruct for the exact value. In the reconstruction by filtered back projection, the intensity is smeared along the line of projection (figure 3), and the value is combined to form the original object (figure 4). The high attenuation coefficient leads to a high intensity in projected images; hence, the smeared value along that line is high and when combined becomes higher than the rest. Since the attenuation is also smeared onto the air, the boundary becomes blurred. As depicted in yellow boxes of figure 4, some parts of the air have the intensity not less than the object. It is known that the blur has the characteristic function of $\frac{1}{r}$, so the deblurred filter, which is the ramp filter (the blue line in figure 5), is included in the reconstruction. The filter is linear, so it can be added either before or after the back projection. The ramp filter introduces the negative projected intensity; consequently, the intensity of the air region is reduced.

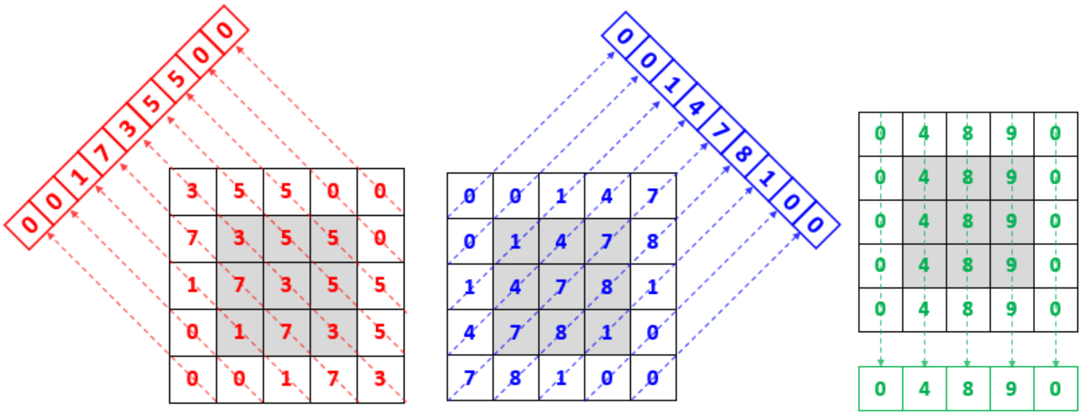

Figure 3 The back-projected images of the projection in figure 2

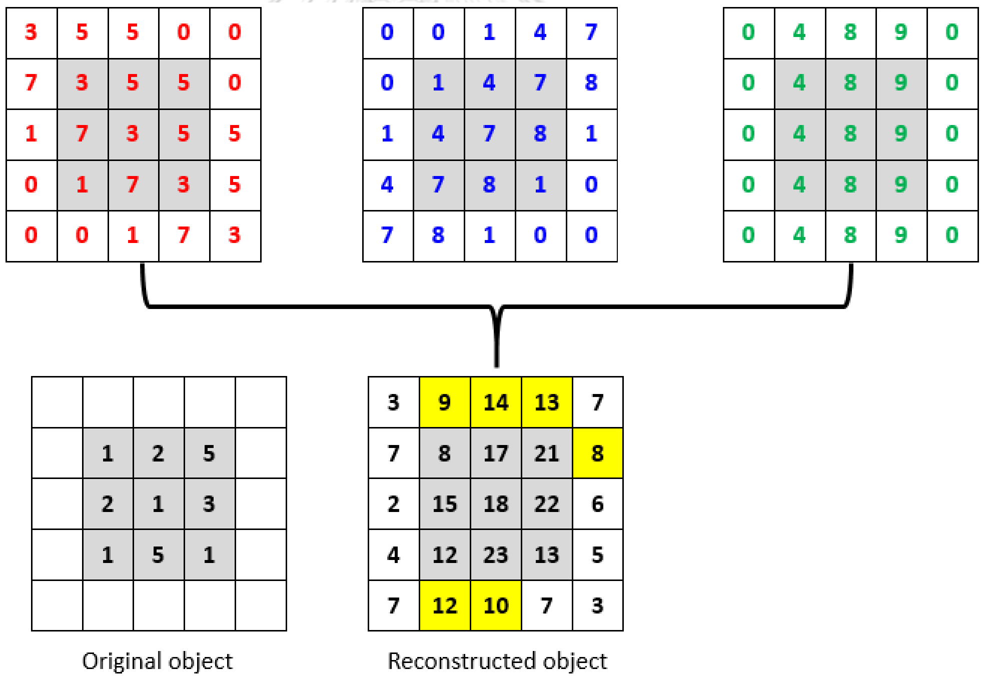

Figure 4 The object reconstructed to form the three projection images by applying back projection. The yellow box depicted the blurred parts.

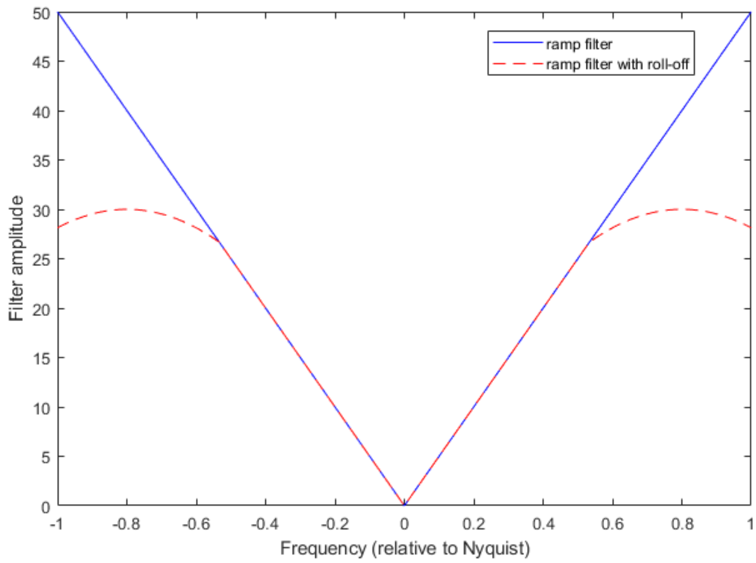

Figure 5 The transfer function of the ramp filter

Most noise is in the high-frequency domain. Since a ramp filter has high gain at high frequency, the noise is amplified. To reduce the effect of the noise, its response is attenuated at high frequency as depicted in red in figure 5. However, if the noise is high, the roll-off is not sufficient to suppress its effect and lead to the incorrect reconstruction.

2.4 Reconstruction in practice (1)

Although the very first computed tomography system used an iterative reconstruction algorithm based on algebraic reconstruction, nowadays the standard reconstruction on almost all computed tomography systems is analytical. This is mainly because analytical reconstruction is a one-step procedure which is much faster than iterative reconstruction. Analytical reconstruction assumes an ideal model. In an ideal model, the reconstruction volume consists of points (that are presented as voxels for displaying images), and projection lines are infinitely thin lines connecting a point source with a point detector element. Moreover, in ideal systems, the measurements are assumed to be real projections of the distribution function without noise.

Under most circumstances, computed tomography measurements are relatively close to ideal. The reconstruction volume is well sampled, and the photon flux is high which results in somewhat low noise. Analytical reconstruction only starts to introduce artifacts in the images when these criteria are violated to a greater extent. This happens for example when the photon flux decreases, and the measurements have higher noise levels. Analytical reconstruction will still treat the measurement as if it was noise free, giving equal importance to rays with high and low noise. This typically results in streaks over the image. Analytical reconstruction is also sensitive to an insufficient or incomplete sampling of the Fourier space. This happens for example when the angular sampling of the object is coarse or incomplete, or when parts of the object are not visible for the detector under certain angles, often called truncation. Under such circumstances, analytical reconstruction will introduce artifacts in the image.

The advantage of iterative reconstruction in computed tomography, compared to analytical methods, is the possibility to work with transmission data rather than log-converted data. This allows using Poisson statistics for the data. Moreover, the log-conversion can become (computationally) unstable for low intensities. To avoiding, low data points are often artificially increased to a certain point where the logarithm becomes stable. By applying the log-conversion for very low intensities, a positive bias can be introduced to keep the logarithm stable.

The major computed tomography vendors today have an option to install iterative computed tomography reconstruction on one or more of their systems. However, very few of them implemented accurate iterative reconstruction as explained above. The main reason is that going back and forward from the projection domain to the image domain is extremely computationally demanding. Usually, only an approximated iterative procedure that stays in the image domain is implemented, with in some cases a few feedback loops to the projection domain. As an example, a typical whole-body computed tomography scan is more than 1 GB; the corresponding reconstruction is less than 300 MB. Full iterative reconstruction for computed tomography would still take a long time, and this is not acceptable for routine clinical usage. In research environments, many iterative reconstruction algorithms for computed tomography have been developed. In the research arena, both monochromatic and polychromatic algorithms are studied. Their advantages over analytical reconstruction and possibilities for acceleration are investigated.

2.5 The metal artifact in computed tomography (14)

Computed tomography has been strongly evolved since its invention. Under most circumstances, computed tomography delivers high-quality images, with relatively high resolution and few artifacts. An essential cause for image degradation is the presence of metals with high attenuation such as metallic implants and dental fillings. The artifacts typically appear as mostly in the bright and dark area and shadows that mask underlying structures. This often hinders proper evaluation and diagnosis in the affected region that is shown in figure 6. The significant results of metal artifacts are photon starvation, scatter, beam hardening, partial volume effects and noise. In figure 7, an overview is given of the effect of the metal artifacts separately. The reconstructions have been performed with filtered back projection.

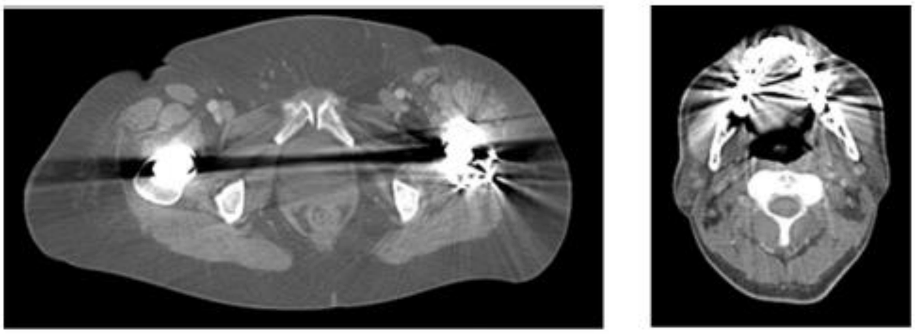

(a) (b)

Figure 6 Example of a computed tomographic image with metal artifacts. (a) patient with two femoral (hip) prostheses. (b) patient with dental fillings.

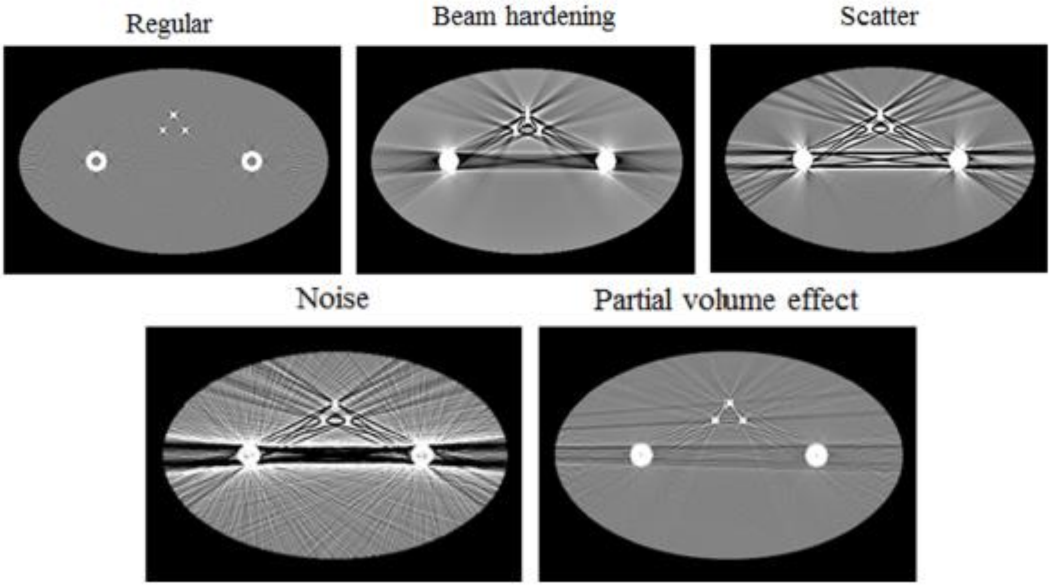

Figure 7 Simulation and reconstruction for the different results of metal artifacts. The reconstructions are performed with filtered back projection.

2.6 Beam hardening

The X-ray photons used in computed tomography have a broad spectrum of energies. When passing through an object, the lower energy photon will more likely be attenuated. This makes that the mean energy of the beam increases and the relationship between total attenuation and object length becomes nonlinear, that is shown in figure 8. This effect is not incorporated in most reconstruction algorithms. Instead, a linear behavior is assumed.

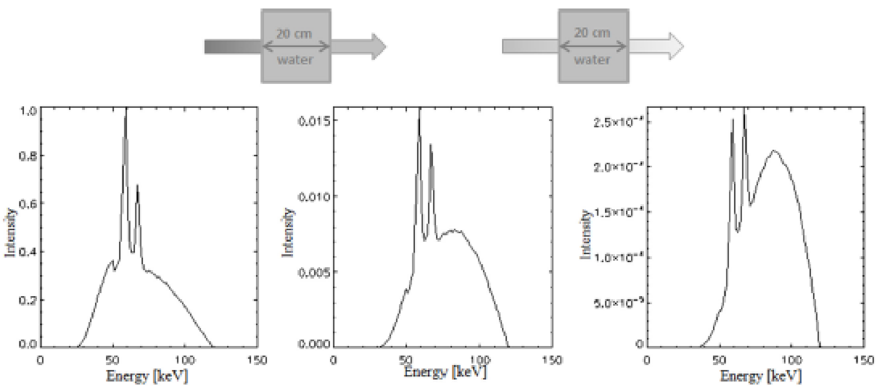

Figure 8 Hardening of the x-ray spectrum. A spectrum of x-rays is sent through 20 cm and 40 cm of water. The resulting spectrum is harder than before.

For objects with relatively low attenuation, this leads to cupping. Cupping is shown in figure 7 where the reconstruction without sinogram correction has lower attenuation values towards the center of the object. The central mechanism of the cupping artifact is the beam hardening effect. When the x-ray beam is passing through the medium, it affects to the beam energy. The profile is differing from the calibration. Typically, the sinogram data are pre-corrected for this effect. If one assumes that the object contains only one material (in clinical applications this is water or soft tissue), a polynomial can be created that links the resulting total attenuation for a polychromatic source with the attenuation that would be obtained for a monochromatic source. In figure 9, a reconstruction based on sinogram data with and without precorrection is shown. For water, this correction is correct; other materials are only partially corrected depending on the difference in their attenuation properties compared to water. Most metals attenuate much more radiation than water and even when applying the water precorrection the metal value is still far from the real value. When beam hardening is not reasonably incorporated in the reconstruction algorithm, severe artifacts may appear. These artifacts are typically dark streaks and shadows around and in between metal. The dark area of metal streak artifact due to beam hardening effect could be avoided by incorporating energy-dependent attenuation coefficients in the reconstruction model. When the metal object attenuates so strongly that no photons remain, the term photon starvation is used. In this case, no information about the projection lines through the metal is obtained. These results are incomplete tomography with stronger artifacts than for beam hardening with remaining photons.

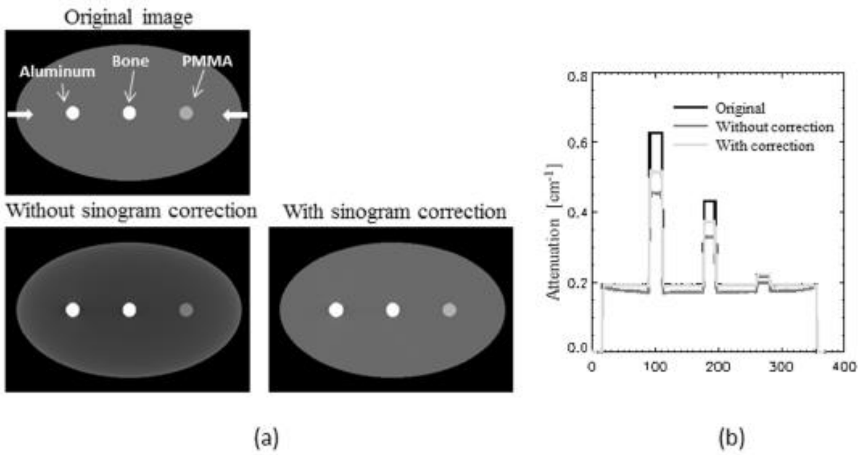

Figure 9 Effect of sinogram beam hardening and cupping correction the reconstructed attenuation values.

2.7 Scatter

When a photon is attenuated, it is assumed to be removed from the x-ray beam by most standard reconstruction algorithms. This is correct if it is attenuated via the photo-electric effect but during Compton scattering secondary photons are produced. When the angle of the deviation is such that the photon stays within the beam, it can be detected and contaminates the measurement. For relatively low attenuating objects this again results in cupping. When highly attenuating objects, like metals, are present in the field of view more severe artifacts can arise, typically dark and white streaking. The projection through the metal receives only a few photons, when photons from neighboring structures scatter into the metal projection rays, a significant increase in detected photons is achieved, that is shown in figure 10.

An effect of scattered photons can be reduced by hardware and software solutions. In clinical multi-slice systems, an anti-scatter grid is placed on top of the detector. Scatter can also be corrected afterward by object-dependent Monte Carlo simulations. Based on an initial reconstruction, the percentage of attenuation due to Compton scatter is estimated by a Monte Carlo simulation and the number of scattered photons reaching the detector is estimated. The obtained scattered profile can be subtracted from the measurement or included in a forward projection model to reduce artifacts in the image. This procedure is not applied on a routine basis since accurate Monte Carlo simulations are very time consuming

.

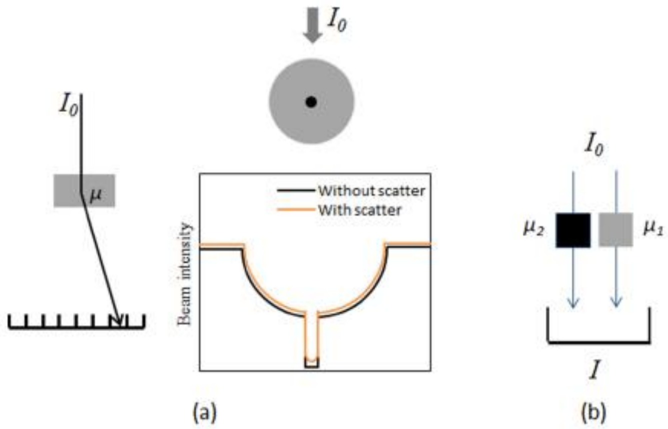

Figure 10 (a) Effect of Compton scatter. The relative effect of scattering will be more significant in metal projection. (b) Partial volume effect.

2.8 Partial volume effects

Partial volume effects in computed tomography are two-sided. A linear effect, also seen for other imaging modalities as in PET, is when the volume represented by a voxel is occupied by two materials with different attenuation properties. The resulting attenuation for that voxel will be a volume-averaged attenuation. However, the exponential nature of computed tomography measurement makes the effect nonlinear. Integration of the beam width, focal spot and projection views (in case of continuous rotation) gives rise to nonlinear partial volume artifacts. These artifacts are fine streaks connecting material boundaries, and they are more pronounced when two neighboring materials have a substantial difference in attenuation.

2.9 Noise

Poisson photon noise caused by the quantum statistical nature of an attenuation event is considered the most dominant. It appears as small dots in the images. As with scatter, small changes in low projection values have a significant influence and give rise to artifacts. Projections through metals have low intensity and noise will have a more extensive influence than for other projection rays. For small metals, this results in fine streaks connecting the different metals, for more significant metals the streaking is stronger causing dark bands in between the metals. Detection related noise is often not considered. However, for measurements of only a few photons, it might also be important.

The noise in computed tomography presents in all electronic systems from some sources including electronic interference. This noise is the irregular pattern in computed tomographic images. It could reduce the image quality in clinical practice. The quantum noise in computed tomography depends on the number of the signal from x-ray photons going to the detector. The source of noise is the detector system and the reconstruction kernel. Noise in the computed tomography can be decreased by increasing the tube-current time, mAs or changing filters during reconstruction.

The attenuation coefficient between the voxel is the other source of the noise in CT. In computed tomography, the attenuation coefficients of the individual tissue voxels are measured. If we have two voxels of the same tissue, we would expect to measure identical attenuation coefficient values, and when these are translated into computed tomography numbers, we would expect to get similar numbers, in reality, it is not. To evaluate noise, a computed tomographic image of the water tank is acquired. Water is homogeneous and has a definite computed tomography number of zero. However, a computed tomography scan of water reveals variations in pixel brightness because of the noise.

Noise can be quantified when we count the number of pixels within a region of interest followed by the statistical analysis of the various computed tomography numbers; the resultant statistical distribution would most likely be a bell-shaped curve. The amount of spread or deviation can be evaluated by determining the standard deviation, which is the easiest and excellent way of quantifying the amount of noise in computed tomography images. Most computed tomography systems have the software capability of defining a region of interest and calculating the standard deviation.

The mathematical filters selected in the image reconstruction process can also be used to control noise. Typically, 10 to 12 filters with different characteristics are commercially available. The smoothing filters are used to reduce noise. Unfortunately, as the noise is reduced by using a smoothing filter, the blurring and decrease the visibility of detail in the image would be obtained. The edge-enhancing or detail-enhancing filter with essentially an opposite characteristic is available. A filter of this type might be selected when the primary goal is a visualization of small detail. Computed tomography manufacturers recommend specific filters for specific clinical procedures.

The quantum noise in computed tomography may be decreased by increasing the number of photons absorbed in each voxel by increasing mAs, slice thickness, and the pixel size. In clinical practice, when increasing the mAs, it is sufficient for the patient dose. To optimize the patient dose and image quality, the radiologist could accept the more noise picture consistent with the proper diagnosis.

Reducing the acquisition time and reducing the slice thickness also involves an increase in noise. However, the mA is increased proportionally. There is a deficiency of photons and noise is accordingly worse with thicker patients and also when there are high-attenuation materials such as bone or prostheses in the slice.

2.10 Metal artifact reduction for orthopedic implant (OMAR) (13)

OMAR is the commercial of metal artifact reduction technique. It is a product from Philips Healthcare. OMAR implements a robust and efficient method to alleviate artifact caused by metal objects from the orthopedic implant in CT images. The crux of OMAR is the iterative method in the reconstruction process in computed tomography. It used the concept of the subtracted image from the original image with streak artifact. The concept of OMAR technique is shown in figure 11.

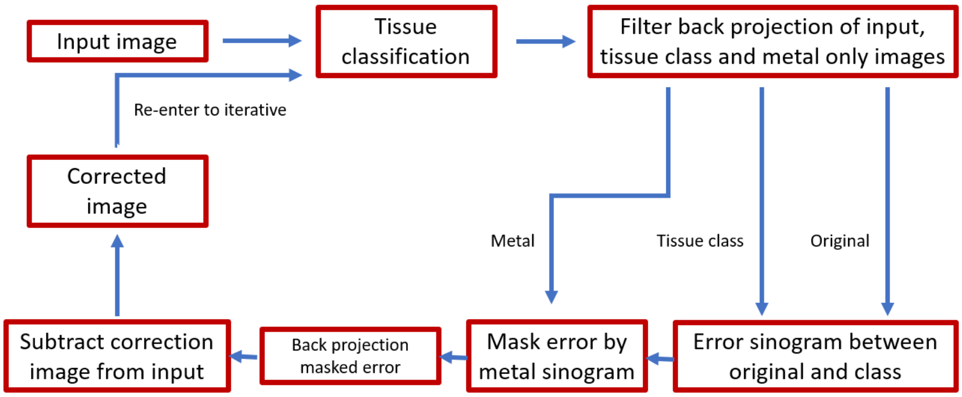

Figure 11 A system diagram of metal artifact reduction for orthopedic implant

The primary purpose of the OMAR algorithm is to correct the streak artifact due to an orthopedic device that implanted in healthy tissue. However, when implementing the OMAR in clinical practice, in some cases could induce the new minor artifact in the computed tomography. The common problem of OMAR technique will appear when the metal is near low-density tissue.

The contraindication of OMAR is the metal near the low density such as air or lung and with iodinated contrast. Pacemaker, dental filling with amalgam and metal screws in the spine could be a significant problem in OMAR method. These are the limitation of OMAR method because, after reconstruction by OMAR, it can induce the new significant artifact in the computed tomographic images.

2.11 Literature review

Lecchi M et al. (15) reviewed the current concept of imaging in radiation therapy. They indicated that CT is the primary imaging modality for tumor and normal healthy tissue delineation and dose calculation in the treatment planning system. Magnetic resonance imaging (MRI) should be used for delineation of the central nervous system tumors and prostate cancer; some studies reported the consistency of quantitative delineation improvements of up to 80% in tumor volume definition.

The positron emission tomography (PET) is the imaging modality in the oncological biomarker. However, they said that the limitations of CT imaging are soft tissue contrast, metal streak artifact due to a metal implant in the body.

Boas EF et al. (3) and Barrett et al. (2) reviewed the causes type and source of artifact in CT. They described that the artifact of CT could severely degrade the image quality and result in making diagnostically unusable. The common artifact can separate into three types: physics-based, patient-based and scanner-based artifacts. One of the most common artifacts in CT that they describe is the metal artifact. The mechanism of metal artifacts may cause by photon starvation, scatter, beam hardening effect, and quantum noise. The metal deletion technique (MDT) that proposed by Boas EF et al. is used in the iterative reconstruction technique to suppress the streak artifact due to metal in CT imaging. This technique can reduce the metal artifact caused by all sources of artifacts. They showed that in some cases, it could improve the image quality.

Mouton A et al. (16) , Kak AC et al. (17) , Hsieh J et al. (8) reported a preliminary survey of metal artifact suppression in CT. Metal artifact reduction (MAR) is the generic name that used for suppressing the streak artifact in CT. Many techniques and method in the literature include photon counting noise, beam hardening correction, Algebraic reconstruction technique, Noisy projection data, and linear interpolation technique. The method of photon counting noise is increasing the tube current in the x-ray source. In clinical practice, this technique is not accessible because when tube current is increased, the dose to the patient also increases. This technique mostly used in the industrial factory. The beam hardening correction is applied the iterative based on the correct reconstructed image. The algebraic reconstruction technique is modified to coverage to maximum likelihood, maximum entropy or minimum norm solution. The noisy projection data is replacing with smoothed or interpolated data from original data. The linear interpolation technique, this technique is erasing the metal by overriding the rays that pass-through metal with values linearly interpolated from rays that pass adjacent to the metal, then uses filtered back projection to reconstruct the image.

Lewis M et al. (18) presented the new technique for metal artifact reduction in CT. This technique tries to rotate the gantry and using the multiplanar reformation until metal artifact decreased. This technique mostly used in the experiment in the object but not practical in the clinical. They showed that it could suppress the metal artifact in knee prostheses when using the appropriate the angles and reformation technique.

Man BD et al. (4, 5) presented a novel technique for metal artifact suppression in CT. They studied the new technique in the phantom when applying their method. Their study compared the results of their approach to those obtained by an iterative method that ignores projections through metal and projection completion method. The performance of new metal artifact reduction is based on the transmission maximum-likelihood algorithm using a-prior knowledge and using an increased number of degrees of freedom.

Yu H et al. (11) proposed a new segmentation-based interpolation method to reduce the metal artifacts caused by a surgical clip. This method consists of five steps: coarse image reconstruction, metallic object segmentation, forward-projection, projection interpolation and final image reconstruction. They studied ion both phantom and patient data sets. The result of their study indicated that could reduce the metal artifact by 20 to 40% according to the standard deviation around the surgical clip.

Joemai RMS et al. (19) developed, implemented and compared two metal artifact reduction methods for CT. They compare the Radon transformation of the computed tomography images, forward projection of the computed tomography images and applying corrections in the scanner specification. They study in four patients with shoulder prosthesis. They also tried to develop the method to analyze the quantitative analysis that compares the image quality for two metal artifact reduction techniques. The result of their study showed that metal artifact suppression technique using either of the two methods yields a reduce the noise and artifact in computed tomography images. Quantitative analysis of clinical practice images demonstrated improved image quality for both techniques of metal artifact reduction.

Boas FE et al. (3) evaluated the metal deletion technique and others reconstruction technique for suppressing the metal artifacts in computed tomographic images and compare these techniques with the conventional algorithm in clinical practice and linear interpolation techniques. They studied in the simulation projection phantom and patient with a metal implant. The computed tomographic images were reconstructed by four methods; filtered back projection, linear interpolation, selective algebraic reconstruction and metal deletion techniques. They used the average error for quantitative analysis. The simulation showed that metal deletion technique suppressed the metal streak artifacts caused by photon starvation, and beam hardening. However, the limitations of metal deletion technique did not address in beam hardening, limited field of view reconstruction. The MDT was tested with a single CT scanner and not tested with a helical pitch higher than 1. The other limitation of MDT is the reconstruction time. It is 19 times slower than FBP.

Koehler T et al. (20) proposed the new technique for metal artifact suppression in CT. It is the sinogram interpolation technique. The method further comprises an adaptive application of the correction image which is uniquely designed to avoid the metal artifact and non-introduce the new artifacts in CT images. This studied is using a couple of clinical data cases. They contributed the basic metal artifact reduction algorithm that works well already in most cases and the idea of adaptive application of the correction image, which is specifically designed to avoid the introduction of new artifacts in the image after application of metal artifact reduction.

Li H et al. (21) studied the effectiveness of the OMAR in radiotherapy application and evaluated the clinical applications in treatment planning both phantom and clinical data of OMAR. They studied ten computed tomography image sets of patients with the orthopedic implant in the hip. The result of the phantom study showed that CT number accuracy and noise were improved on OMAR corrected images, especially for images with bilateral hip implants. In all patient cases, radiation oncologist scored OMAR corrected images as higher quality in term of artifact reduction. The overall image quality and the clear of normal structures were significantly improved compared with the FBP images. They conclude that this experiment demonstrated that OMAR could reduce metal artifacts and improve CT number accuracy and target and normal structure delineation. However, the limitations of OMAR are metal near air or low-density tissue, pacemakers, screw in the spine and dental filling.

Oonsiri S et al. (22) , Giantsaoudo D et al. (23) , and Hansen CR et al. studied the image quality and dosimetry using metal artifact reduction techniques in the treatment planning system. a They found that the delineation of structure in the head and neck were affected by metal reduction techniques. It showed more consistent after the metal artifact reduction applied. However, only small changes were observed in dose calculation in the treatment planning. For intensity modulated radiation therapy (IMRT) and volumetric modulated arc therapy (VMAT), the dose calculation difference between the filtered back projection technique and applied metal artifact reduction was 0.2 ±1.4 cGy.

Wagenaar et al. (24) reported the difference in the performance of the available metal artifact reduction techniques of different scanners and comparing to the metal deletion technique. Philips, GE, and Siemens were requested to use their optimized computed tomography scanner for applying their metal artifact reduction techniques. This studied was using an anthropomorphic head and neck phantom in the experiment. Three amalgams were inserted between the phantom's teeth. The average absolute error was analyzed for all reconstructions in the amalgam implants. This studied showed that metal deletion technique showed the best over the three commercial metal artifact reduction techniques both in the qualitative and quantitative analysis.

Anderla A et al. (25) and Park PC et al. (26) proposed a new technique for metal-artifact suppression by magnetic resonance imaging information in the artifact region. These methods tried to encounter the way to suppression the streak with the intensity of the MRI. The new algorithm corrects reconstructed computed tomographic images by mapping computed tomography Hounsfield units from an adjacent slice, using a registered magnetic resonance image. The results indicated that the new method was suppressed the severe metal artifacts without created the new artifacts. They concluded that magnetic resonance image based computed tomography artifact correction method could improve computed tomographic image quality in the computed tomographic images.

Chapter 3
Research methodology

3.1 Research question

What is the method to suppress the metal artifact in computed tomography images at the head and neck region?

3.2 Research objective

The purpose of this study is to develop the method for metal artifact reduction in computed tomography imaging at head and neck using MATLAB software.

3.3 Scope

The study focuses the method for suppression of metal artifact in the computed tomography images in head and neck region.

3.4 Research design

This study has been designed as a descriptive observational study.

3.5 Research design model

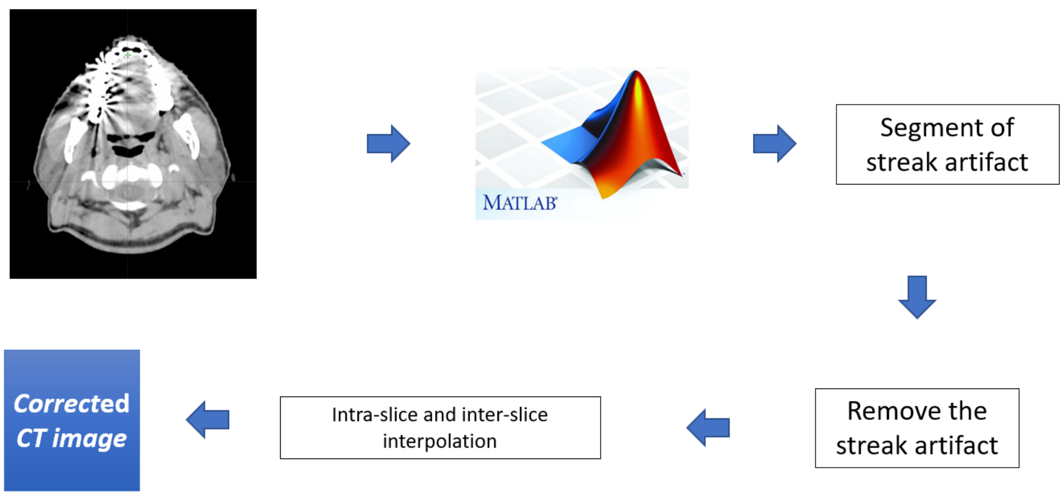

3.6 Conceptual framework

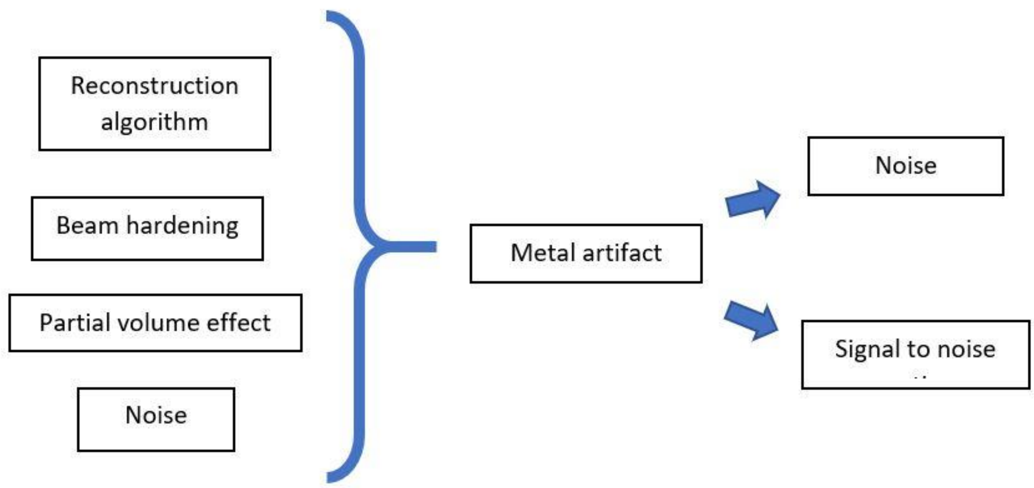

3.7 Material

1. Computed tomography scanner

Philips Brilliance Big Bore computed tomography simulator is the 7th generation of sixteen slices helical computed tomography scanner. Philips Brilliance Big Bore oncology configuration provides powerful tools to improve patient care and increase daily throughput. The 85 cm bore diameter, and actual 60 cm scan field of view enables to scan cancer patients with immobilization devices, patient monitoring devices, intravenous delivery devices, and motion management system device. Commercially OMAR (13) supports the image quality needs of the radiation therapy department. Philips Brilliance Big Bore oncology is shown in figure 12.

Figure 12 Philips Brilliance Big Bore computed tomography simulator

2. MATLAB (27)

The MATLAB platform is optimized for solving engineering and scientific problems. The matrix-based MATLAB language is the way to express computational mathematics. Built-in graphics make it easy to visualize and gain insights from data. A vast library of prebuilt toolboxes gets started right away with algorithms essential to its domain. The MATLAB desktop is the main MATLAB application window. The desktop contains five subwindows: the command window, the workspace browser, the current directory window, the command history window and one or more figure windows, which are shown only when the user displays a graphic. The MATLAB version R2012 was used in this study.

3. Computed tomography dose index head phantom

The computed tomography dose index head phantom is made of PMMA at 16 cm diameter cylinder. The length of the phantom is 14 cm. The cylindrical phantom contains five 1.3 cm diameter holes and 10 cm depth for the pencil ion chamber inserted to measure the CTDI in phantom. One hole is set at the center of the cylinder, and four holes are at 90-degree apart, the hole centers are 1 cm from the edge of the cylinder. Computed tomography dose index head phantom includes 5 PMMA jigs inserted 5 holes and phantom support. The computed tomography dose index head phantom is shown in figure 13.

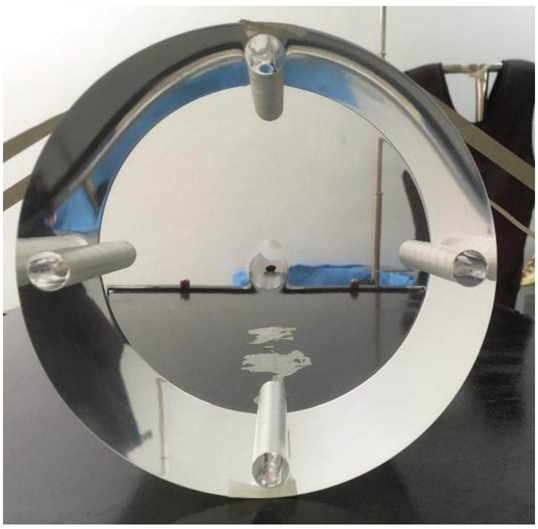

Figure 13 Computed tomography dose index head phantom

4. Alderson Rando phantom

Alderson Rando phantom incorporates materials to simulate various body tissue-muscle, bone, lung, and air cavities. It is made of tissue equivalent material based on synthetic isocyanate rubber. The phantom material is processed chemically and physically to achieve a density of 0.985 g/cm^3 and an effective atomic number of 7.3 based on the International Commission on Radiation Units and Measurement (ICRU). The Alderson Rando phantom is shaped into a human and sectioned transversely into slices of 2.5 cm thick, each containing a matrix of 0.5 cm diameter holes spaced 3 cm apart. The head region of Alderson Rando phantom is shown in figure 14. In this study, only the head region of the Alderson Rando phantom is used.

Figure 14 Left: The head region of Alderson-Rando phantom Right: One transverse-axial slab

5. Computed tomography images with metal artifact

The computed tomography images of head and neck patient with a metal artifact at the Division of Radiation Oncology, Department of Radiology, King

Chulalongkorn Memorial Hospital were included in this study. The computed tomography images of head and neck patient are shown in figure 15.

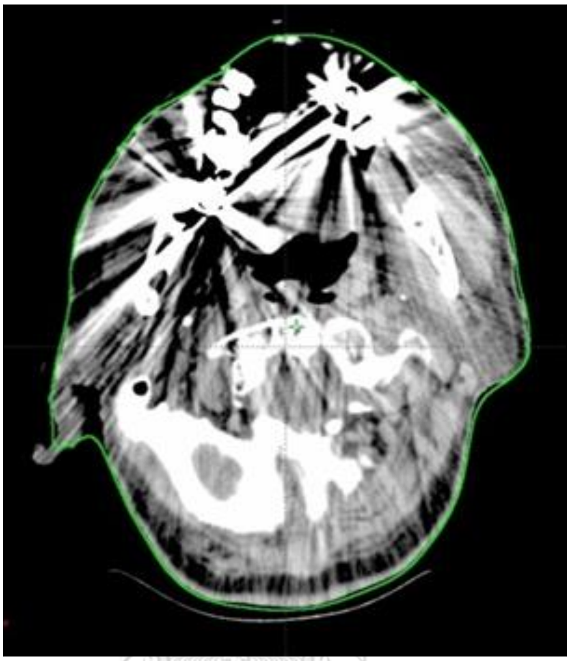

Figure 15 Computed tomography image of a patient with the metal artifact in the head and neck region.

3.8 Method

1. Develop and improve methods for suppression of metal artifacts in computed tomography images.
    a. The new metal artifact reduction method has been developed to improve images containing metallic artifact. Computed tomographic image from filtered back projection was used as the original image.
    b. The concept of the algorithm was the B-spline and averagely weighted interpolation technique.
2. Verify new method in homogeneous and Alderson Rando phantoms
    a. Once the new metal artifact reduction optimization phase was completed, homogeneous and Alderson-Rando phantom images

were tested and evaluated using the new method with and without metallic inserts.

b. The tube voltage was fixed at 120 kVp and vary tube current-time at 100, 150, 200 and 250 mAs for all phantom studies.

c. The acquisition was repeated three times per mAs settings.

3. Implement the new method to the patient computed tomography images.

   a. The fifty-two images from head and neck cancer patients with metal artifact images from computed tomographic images were subjected to the metal artifact reduction methods.

4. Evaluate the image quality.

   a. The efficacy of the metal artifact reduction algorithm was assessed using quantitative and qualitative analysis.

   b. The quantitative analysis of image quality was obtained from percent noise in equation 7. The region of interest in the area of 1 cm^2 in circular shape was placed not too far or too close to the metal artifact region.

$$Percent\ noise = \frac{SD}{Mean} \times 100 \qquad ...8$$

   c. The qualitative analysis performed by two independent radiation oncologists with similar experience score the image quality and rule out the best image among filtered back projection, OMAR, and a new method for metal artifact reduction.

3.9 The sample

3.9.1 Target population

The head and neck computed tomographic images acquired at the Division of Radiation Oncology, Department of Radiology, King Chulalongkorn Memorial Hospital.

3.9.2 Sample

The head and neck computed tomographic images included the metal artifact.

3.9.3 Sample size determination

The sample population is independent, perspective data. The sample size was determined using equation 8.

$$n = \frac{(Z_{\alpha/2} + Z_{\beta})^2 \sigma^2}{d^2} = 41.9 \qquad \text{...9}$$

n	=	Number of sample
$Z_{\alpha/2}$	=	1.96 (@95% Confidence interval of the result)
$Z\beta$	=	1.28 ($Z_{0.10}$)
σ^2	=	Variance of data = $(200\ \mathrm{HU})^2$ (22)
d	=	Acceptable error = 100 HU

3.10 Expected benefits

1. The method to suppress metal artifact in computed tomographic images in head and neck region.
2. Reduction of the metallic artifact in routine clinical images.
3. Improve image quality and diagnostic confidence in the metallic artifact of the head and neck region.

4. Higher accuracy in interpretation of computed tomography images.

3.11 Measurement

Independent variable: Metal artifact reduction method

Dependent variable: Computed tomography number, noise, percent noise

3.12 Data collection

The percent noise determined the image quality. The region of interest in the area of 1 cm^2 in circular shape was placed in the vicinity of the metal artifact region. The data was collected at the Division of Radiation Oncology, Department of Radiology, King Chulalongkorn Memorial Hospital.

3.13 Data analysis

The quantitative image quality of computed tomography images both in phantoms and in patients was reported as mean, standard deviation in the tables. The image quality is defined as the noise and percent noise for each method. The qualitative image quality was determined by two independent radiation oncologists to score the images. Both had the same experience in computed tomographic images interpretation. This study was blind observations for two radiation oncologists, and the weighted Kappa for inter-observer reliability was analyzed by SPSS version 22.

The guidelines of image quality criteria are:

Score 1 = Very dissatisfied

Score 2 = Dissatisfied

Score 3 = Satisfied

Score 4 = Very satisfied

3.14 Outcome

The method to suppress metal artifact in computed tomographic image improves the image quality and diagnostic confidence in the metallic artifact in the head and neck region of cancer patients.

3.15 Statistical analysis

Descriptive statistics: the mean, median, standard deviation, minimum and maximum values of noise and signal to noise ratio were determined by the excel program.

3.16 Ethical consideration

The computed tomography images from patient studies with and without metal artifact were evaluated at the Division of Radiation Oncology, Department of Radiology, King Chulalongkorn Memorial Hospital. This study has already been approved by the Institutional Review Board (IRB), Faculty of Medicine, Chulalongkorn University (IRB 627/60). The certificate is shown in figure 16.

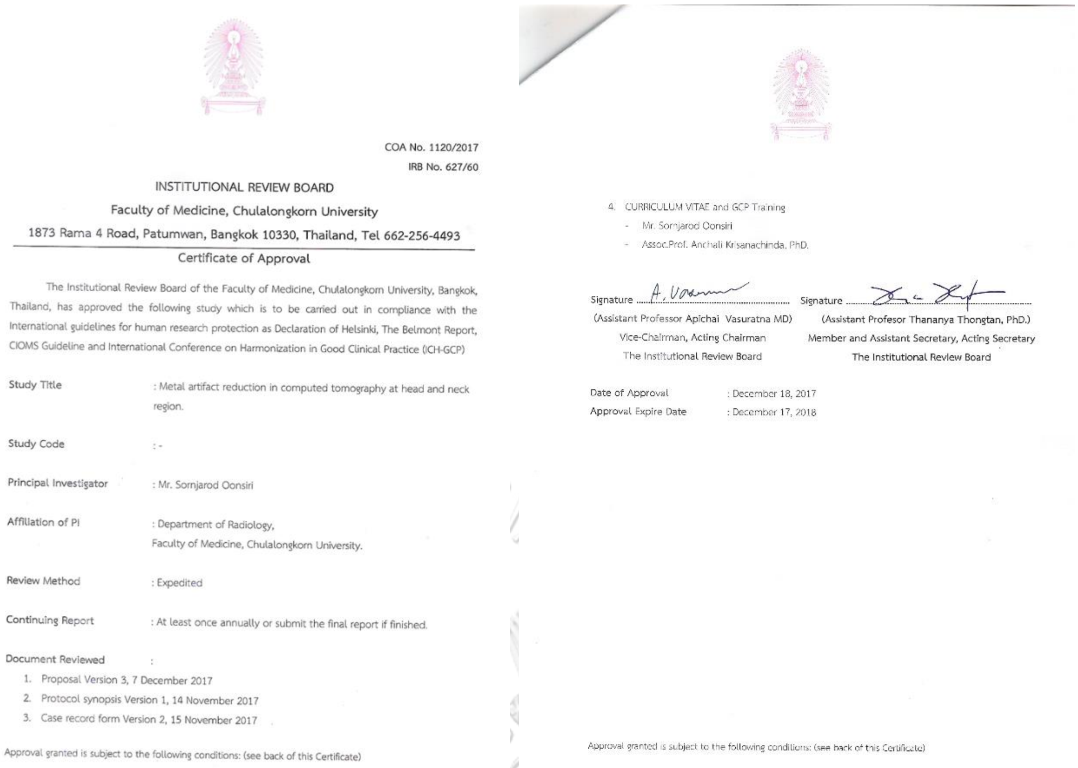
COA No. 1120/2017
IRB No. 627/60

INSTITUTIONAL REVIEW BOARD
Faculty of Medicine, Chulalongkorn University
1873 Rama 4 Road, Patumwan, Bangkok 10330, Thailand, Tel 662-256-4493

Certificate of Approval

The Institutional Review Board of the Faculty of Medicine, Chulalongkorn University, Bangkok, Thailand, has approved the following study which is to be carried out in compliance with the International guidelines for human research protection as Declaration of Helsinki, The Belmont Report, CIOMS Guideline and International Conference on Harmonization in Good Clinical Practice (ICH-GCP)

Study Title	: Metal artifact reduction in computed tomography at head and neck region.
Study Code	: -
Principal Investigator	: Mr. Somjarod Oonsiri
Affiliation of PI	: Department of Radiology, Faculty of Medicine, Chulalongkorn University.
Review Method	: Expedited
Continuing Report	: At least once annually or submit the final report if finished.
Document Reviewed	:

1. Proposal Version 3, 7 December 2017
2. Protocol synopsis Version 1, 14 November 2017
3. Case record form Version 2, 15 November 2017

Approval granted is subject to the following conditions: (see back of this Certificate)

4. CURRICULUM VITAE and GCP Training
- Mr. Somjarod Oonsiri
- Assoc.Prof. Anchali Krisanachinda, PhD.

Signature A. Vasuratna
(Assistant Professor Apichai Vasuratna MD)
Vice-Chairman, Acting Chairman
The Institutional Review Board

Signature
(Assistant Profesor Thananya Thongtan, PhD.)
Member and Assistant Secretary, Acting Secretary
The Institutional Review Board

Date of Approval	: December 18, 2017
Approval Expire Date	: December 17, 2018

Approval granted is subject to the following conditions: (see back of this Certificate)

Figure 16 The certificate of approval from the Institutional Review Board (IRB), Faculty of Medicine, Chulalongkorn University

Chapter 4
Result and Discussion

4.1 Methods for suppression metal artifacts in computed tomography images

The new metal artifact reduction technique has been developed using MATLAB software to improve images containing metal artifacts. The concept of the new method of metal artifact reduction is the B-spline and averagely weighted interpolation techniques. The concept of the new method of metal artifact reduction in the block diagram is shown in figure 17. In clinical, metal artifacts appear in only one or two contiguous transverse axial slices. So, the information lost due to the artifact can be inferred from the slices immediately above and below (inter-slice) as well as within its slice (intra-slice). The information from inter-slices and intra-slice is fused together to estimate the missing information in the new method. Usually, the metal artifact causes very bright and dark streaks in an image so that it can be easily detected by thresholding for the area with very high and low intensities.

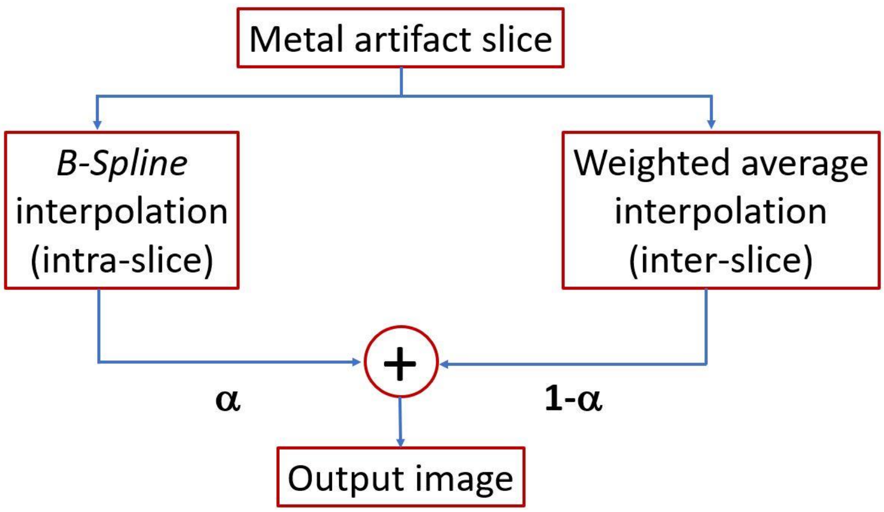

Figure 17 The concept of the new method

The threshold of the streak artifact could be identified in both bright and dark areas in the computed tomographic images by CT number value. The CT number value of computed tomographic images range from -1027 to +3071 HU. Most streak artifact in a bright area, the CT number is higher than +500 HU and the dark area is lesser than 0 HU. After identified the streak artifact in computed tomographic images, these ranges had been implemented. The threshold of the bright area at higher than +500 HU and the dark area inside the body lesser than 0 HU had been fixed, and these areas had been removed.

The B-spline curve (28) is a piecewise polynomial curve whose shape is controlled by control points and the degree of its polynomial basis. The nondecreasing sequence of real number forms a knot vector (U). Control points are assigned the knot which is the element in U and ordered accordingly. The *p*th-degree B-spline curve is defined as follows.

$$\mathbf{C}(u) = \sum_{i=0}^{n} N_{i,p}(u)\mathbf{P}_i, \qquad \text{...10}$$

where C(*u*) is the coordinate of the B-spline curve at the knot value of *u*; (*n*+1) is the number of the control points; P_i is the coordinate of the i-th control point, and $N_{(i,p)}(\cdot)$ is the *i*-th B-spline basis function of p degree. N_(i,p) (·) is iteratively defined as follows.

$$N_{i,0}(u) = \begin{cases} 1, & u_i \le u < u_{i+1} \\ 0, & otherwise \end{cases}, \qquad \text{...11}$$

$$N_{i,p}(u) = \frac{u-u_i}{u_{i+p}-u_i} N_{i,p-1}(u) + \frac{u_{i+p+1}-u}{u_{i+p+1}-u_{i+1}} N_{i+1,p-1}(u) \qquad \text{...12}$$

According to equations 10 and 11, the pth degree basis function is the pth degree polynomial function, whose value is controlled by the positions of (p+1) control points.

A B-spline curve has a strong convex property. It is at least (p-k) times continuously differentiable at $u = u_j$, where k is the number of the controlled points whose knot is assigned the value of u_j. Since the higher order B-spline requires a higher degree of continuity, each control point in the B-spline curve always has only one degree of freedom. Thus, the more control points required to create the curve, the smoother the curve becomes. Figure 18 shows the different degree of the B-spline curve for the same set of control points. The first-order B-spline curve is just the linear line connecting the control points. The higher-order B-spline curve is smoother; consequently, the curve is moved further away from the positions of the control points.

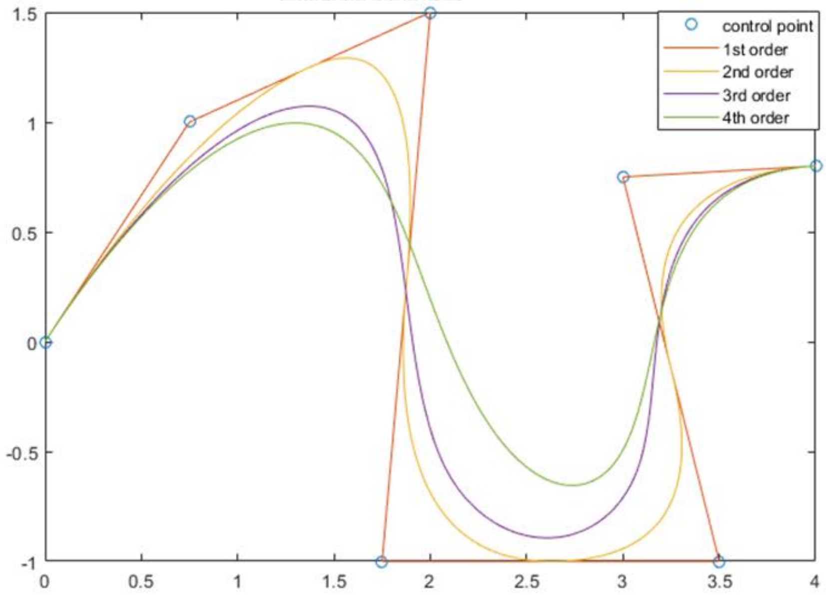

Figure 18 The relationship between the degree of the B-spline curve and the degree of curve smoothing in x and y-axis

The B-spline curve is the continuous curve whose shape is controlled by the discrete number of control points. Thus, it very well suits the requirement of the interpolation problem. It is one of the most popular interpolation methods for signal and image processing. In practice, a signal is uniformly sampled, so the knot is assigned the integer value, where zero represents the signal of interest. The knot vector is fixed, so equations 10 and 11 can be evaluated beforehand. In signal processing, the basis function is derived by the time convolution operation as follows (29).

$$N_0(u) = \begin{cases} 1, & -0.5 < u < 0.5 \\ 0.5, & |u| = 0.5 \\ 0, & otherwise \end{cases}, \qquad ...13$$

$$N_p(u) = N_0(u) * N_{p-1}(u),\ p \geq 1, \qquad ...14$$

where * is the time convolution operator

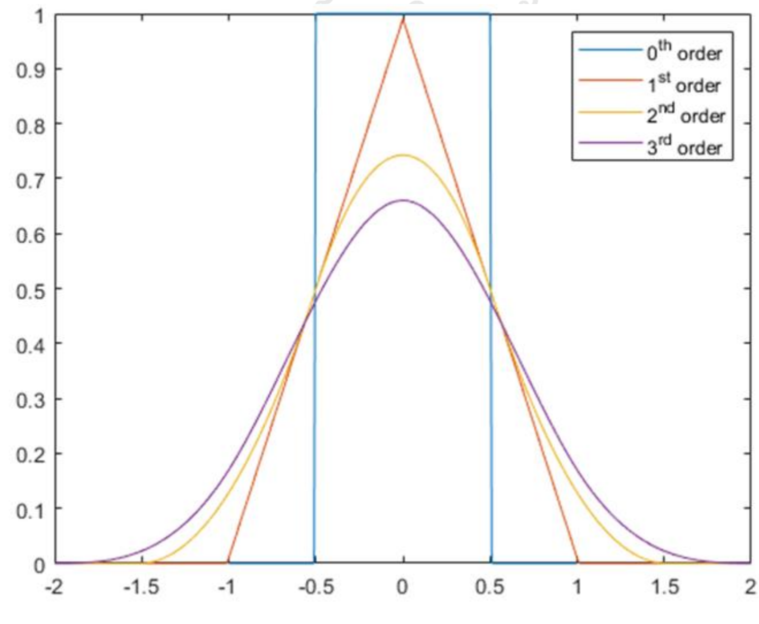

Figure 19 The B-spline basis function for signal interpolation in x and y-axis

Figure 19 shows the basis function for the B-spline interpolation. The 0^{th} and the 1^{st} order functions are used in the nearest neighbor and the linear interpolations, respectively. In signal Interpolation, there is no distinct benefit of using the order of B-spline higher than three. Hence, the 3^{rd} order (cubic) B-spline is the most used interpolation function and evaluated in the closed-form representation as follows.

$$N_3(u) = \begin{cases} \frac{2}{3} - |u|^2 + \frac{|u|^3}{2}, & |u| < 1 \\ \frac{(2-|u|)^3}{6}, & 1 \leq |u| < 2 \\ 0, & otherwise \end{cases} \qquad ...15$$

The interpolation is written in the form of the following linear function (29).

$$s(u) = \sum_{k \in Z} N_p(u-k)c(k), \qquad ...16$$

where s (•) and c (•) are the interpolated intensity and the B-spline coefficient, respectively. The B-spline coefficients are obtained according to the desired interpolation characteristic. For example, if the interpolation curve must have the same intensity as the N available points, they can be obtained by solving the following set of *N* equations.

$$Y(u) = \sum_{k \in Z} N_p(n-k)c(k)\,,\ u = 0,1,2,\ldots,N-1, \qquad ...17$$

where Y(•) is the available intensity.

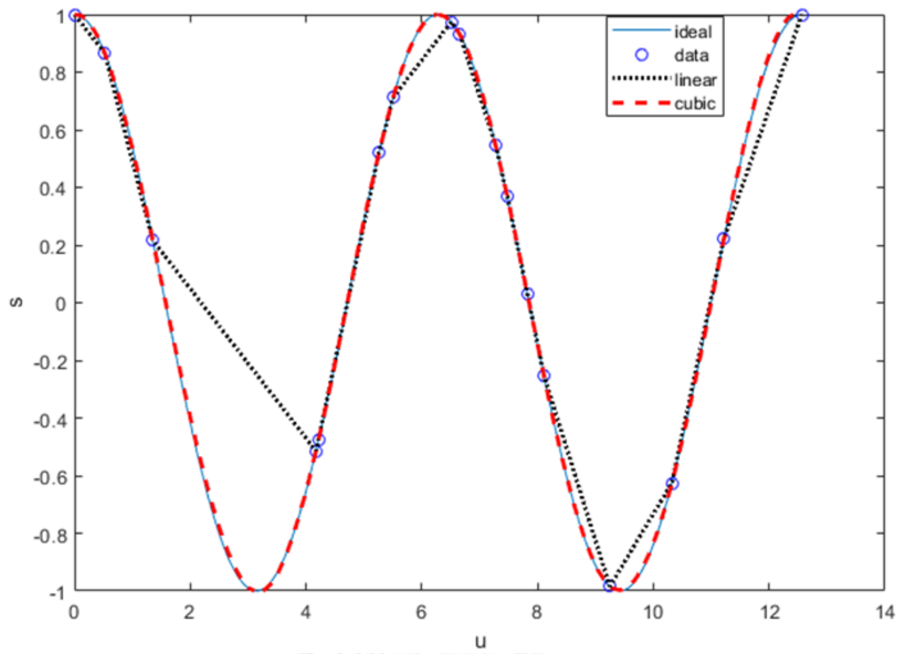

Figure 20 The B-spline interpolation of a noiseless signal

Figure 20 depicts the spline interpolation of a cosine function when only 17 data points are available. The first order interpolation (the dotted line) is the linear interpolation which links given points (circle) by straight lines. The cubic interpolation (the dashed line) is almost exactly the same as the ideal function (the bold line). However, B-spline interpolation is not tolerant to noise. When the given data is noisy, the cubic interpolation (the dashed line) may yield the highly fluctuating intensity as shown in figure 21. In this case, it is better to obtain *c(k)* that is weighted between the linear and the cubic spline interpolation (the dotted line).

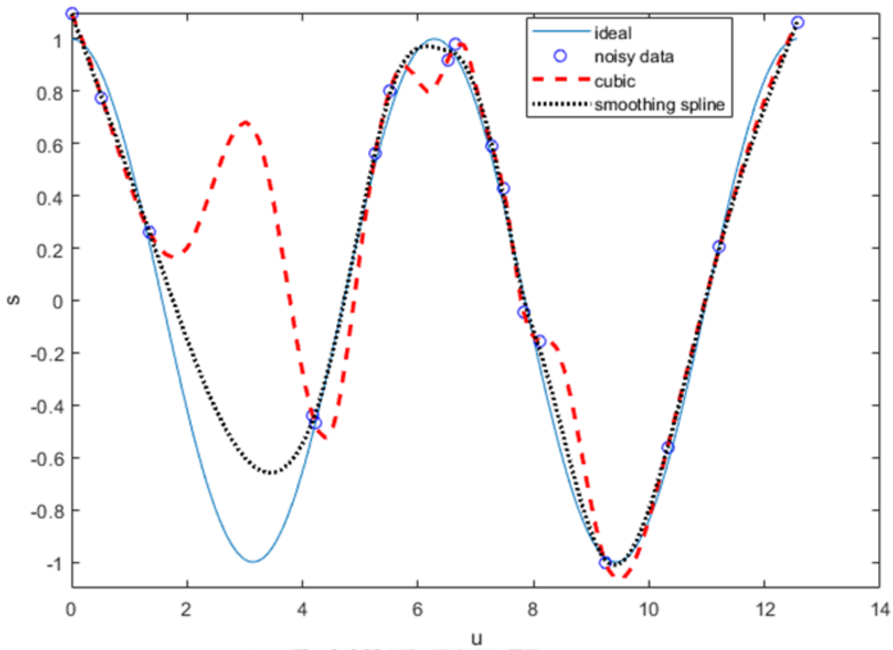

Figure 21 The B-spline interpolation of a noisy signal

Equation 15 can be easily extended to the higher dimension signal by using the tensor product. In case of the image interpolation, the spline interpolation is as follows.

$$s(x,y) = \sum_{l\in Z}\sum_{k\in Z} N_p(x-k)N_p(y-l)c(k,l), \qquad \text{...18}$$

In cubic B-spline interpolation, the range of k that has a non-zero basis in equation 16 is between and including $\lceil x\text{-}2 \rceil$ and ($\lceil x\text{-}2 \rceil$+3). The range of l that has a non-zero basis in equation 16 is between and including $\lceil y\text{-}2 \rceil$ and ($\lceil y\text{-}2 \rceil$+3).

B-spline interpolation is used to find the intra-slice information. The B-spline parameter in this study was 3 for knot and 2 for the degree. The intensity lost by the artifact is interpolated from the intensity within the same slice. The weighted average between the intensities of the slices above and below is used as the inter-slice information. The missing intensity is estimated according to equation 17.

$$I_{interslice,k}(x,y) = \alpha I_{k-1}(x,y) + (1-\alpha) I_{k+1}(x,y) \quad \ldots 19$$

The α variable in equation 18 was fixed to 0.5 in all CT images to avoid the bias in the image processing step. The concept of the new method was a simple and effective method to suppress the metal artifact in the computed tomographic image because the image space-based method in image processing has been used together with DICOM file format from computed tomography. This concept is different from Boas FE et al., 2011 (forward projection metal artifact reduction technique) as it leads to the comparison result with the filtered back projection method.

4.2 Verification of new method in homogeneous and Alderson Rando phantoms

The computed tomographic images with and without artifact using filtered back projection, OMAR, and new method on homogeneous and Alderson Rando phantoms are shown in figure 22, 23, 24 and 25 respectively. The average percent noise of a homogeneous phantom and Alderson Rando phantom with and without artifact of filtered back projection, OMAR, and new method are shown in table 1 and 2, respectively. The percent noise of homogeneous phantom and Alderson Rando phantoms with and without artifact were decreased when the x-ray tube current time, mAs, increased.

The effectiveness of the new method in homogeneous and Alderson Rando phantoms was slightly better than filtered back projection and OMAR methods. The results were consistency when compared with Wagenaar D et al., 2015.

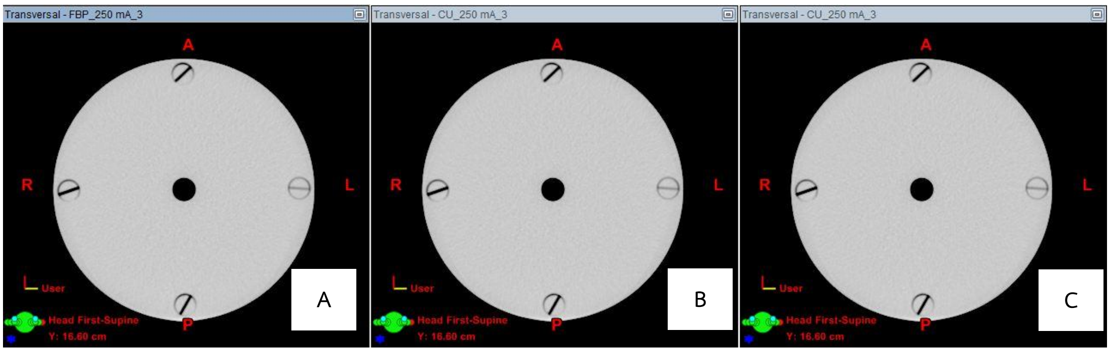

Figure 22 Homogeneous phantoms without metal artifact *A = filtered back projection, B = OMAR, and C = new method*

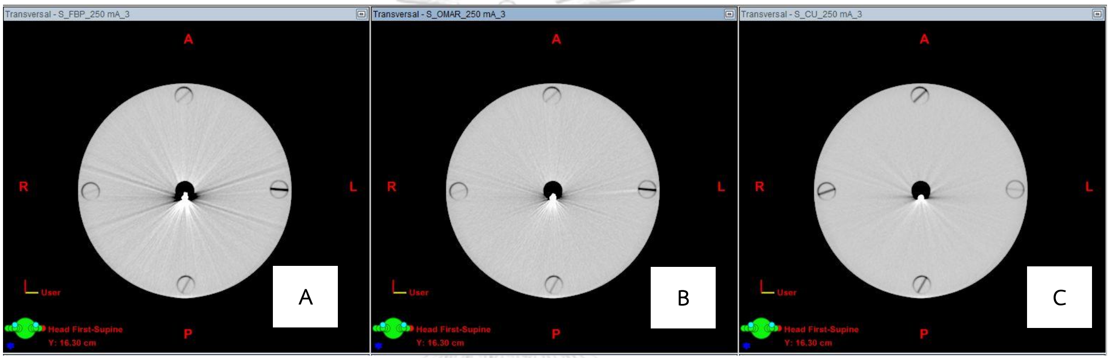

Figure 23 Homogeneous phantoms with metal artifact fixed at center A = filtered back projection, B = OMAR, and C = new method

Table 1 Average percent of the noise of homogeneous phantom with increasing tube current time

mAs	Average %noise (without metal)			Average %noise (with metal)		
	FBP	OMAR	New method	FBP	OMAR	New method
100	8.3 ± 0.6	8.3 ± 0.6	6.4 ± 0.7	34.7 ± 5.3	26.4 ± 2.5	12.1 ± 1.4
150	7.6 ± 0.9	7.6 ± 0.9	5.4 ± 0.2	32.6 ± 3.7	21.2 ± 1.5	12.0 ± 0.3
200	5.9 ± 0.6	5.9 ± 0.5	4.5 ± 0.3	24.8 ± 3.9	19.2 ± 2.1	11.6 ± 1.7
250	5.6 ± 0.5	5.6 ± 0.5	4.2 ± 0.3	23.8 ± 3.6	18.2 ± 1.0	10.5 ± 0.6

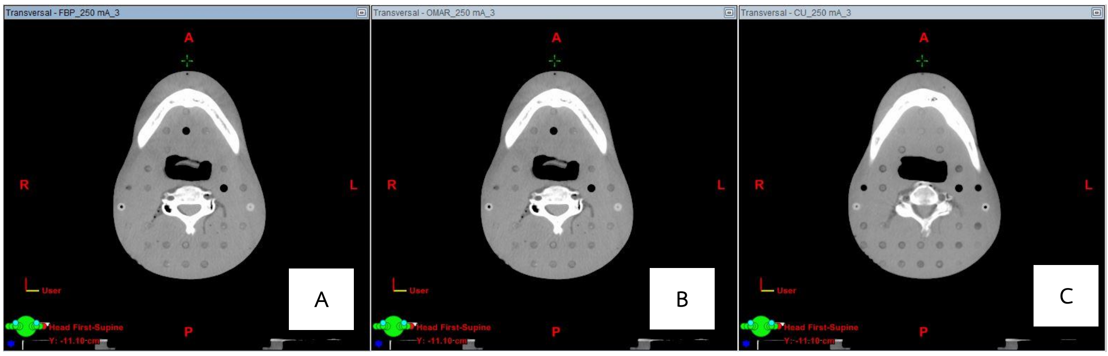

Figure 24 Transverse axial image of Alderson Rando phantom, head and neck part, without metal artifact A = filtered back projection, B = OMAR, and C = new method

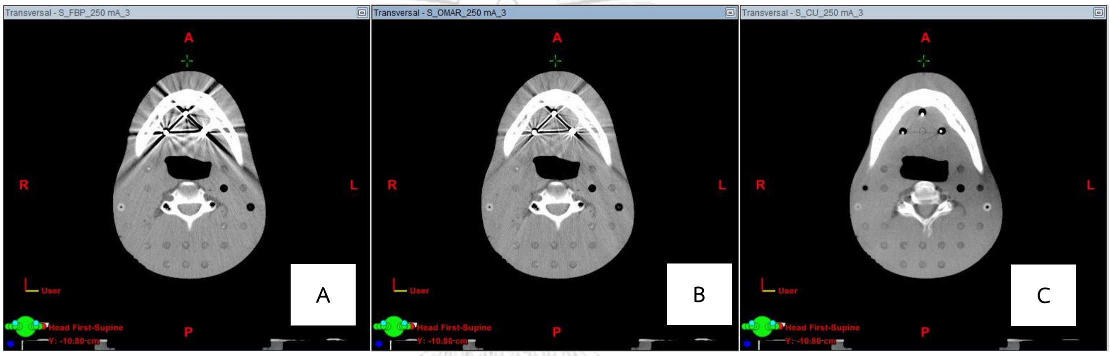

Figure 25 Transverse axial image of Alderson Rando phantom, head and neck part, with metal artifact A = filtered back projection, B = OMAR and C = new method

Table 2 Average percent of the noise of Alderson Rando phantom (HU) with increasing tube current time

mAs	Average %noise (without metal)			Average %noise (with metal)		
	FBP	OMAR	New method	FBP	OMAR	New method
100	66.3 ± 31.0	66.0 ± 30.5	27.9 ± 2.0	290.0 ± 38.7	288.4 ± 22.3	162.6 ± 22.0
150	62.5 ± 38.2	62.6 ± 38.2	22.4 ± 3.2	281.6 ± 44.4	286.8 ± 21.4	105.6 ± 30.0
200	60.1 ± 36.1	59.9 ± 36.2	18.9 ± 1.9	277.3 ± 34.7	283.5 ± 27.6	97.7 ± 31.7
250	54.2 ± 32.1	54.5 ± 32.1	18.9 ± 1.5	264.3 ± 29.6	264.3 ± 28.1	92.4 ± 30.0

4.3 Implementation of the new method to the patient computed tomography images

The example of fifty-two computed tomographic images of head and neck cancer patients with the metal artifact is shown in figure 26. The percent noise of computed tomographic patient images with a metal artifact of filtered back projection, OMAR, and new method are shown in table 3. The average percent noise of computed tomographic patient images of the new method is better than filtered back projection and comparable with orthopedic metal artifact reduction method. Some computed tomographic images of the new method, the image quality is better than filtered back projection and orthopedic metal artifact reduction, but some are worse than filtered back projection and orthopedic metal artifact reduction. The effectiveness of the new method depends on site, size, a number of metallic and image quality of adjacent computed tomographic images.

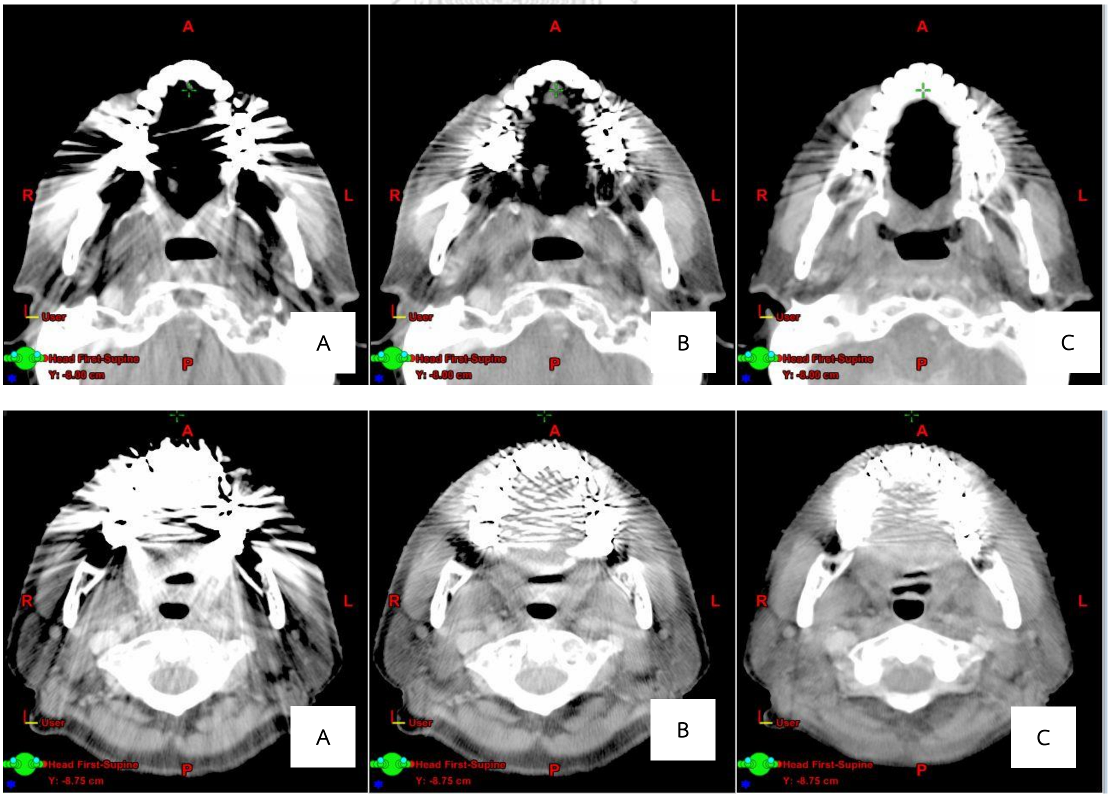

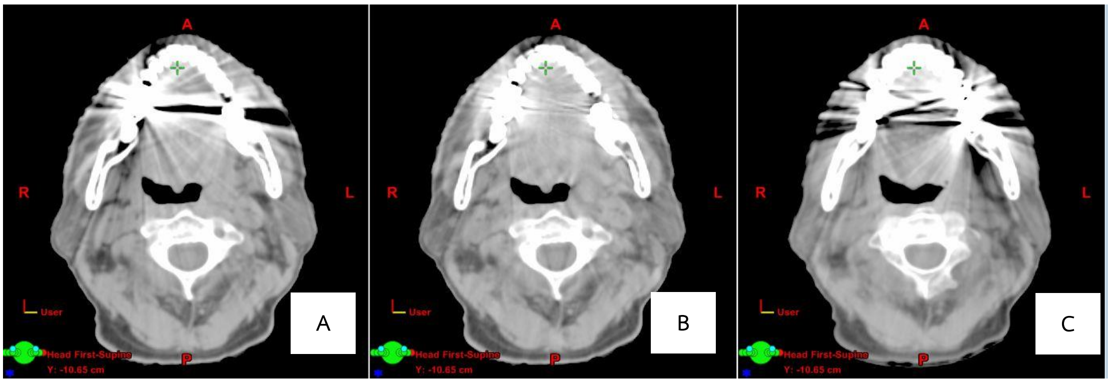

Figure 26 Patient computed tomographic images A = filtered back projection, B = OMAR and C = new method

Table 3 Average percent of the noise of computed tomographic patient images

Average %noise (FBP)	Average %noise (OMAR)	Average %noise (New method)
111.2 ± 65.8	46.6 ± 30.0	63.8 ± 54.7

The performance of both metal artifact method, OMAR and a new method, are shown regarding percent of metal artifact reduction in computed tomographic patient images. It is shown in table 4. The OMAR was slightly at a better result than a new method.

Table 4 The percent of metal artifact reduction in computed tomographic patient images

Percent of metal artifact reduction (%)	
OMAR	New method
55.5 ± 0.15	41.2± 0.23

4.4 The image quality

Two independent radiation oncologists with similar experience evaluated the image quality by scoring the comped tomography images among filtered back projection, OMAR, and a new method for metal artifact reduction. The image quality scoring is shown in table 5. Both radiation oncologist evaluations confirm the agreement on a new method and orthopedic metal artifact reduction offer better image quality than filtered back projection. One of fifty-two computed tomographic images from new method shows more artifact than filtered back projection and orthopedic metal artifact reduction because of many streak artifacts from metal in adjacent slices of computed tomographic images.

Table 5 Image quality of CT images with metal artifacts using three methods, scored by two radiation oncologists (1 = Very dissatisfied, 2 = Dissatisfied, 3 = Satisfied, 4 = Very satisfied)

	Average scores on image quality, with metal artifacts		
	FBP	OMAR	New method
1st Radiation oncologist	1.2 ± 0.4	2.5 ± 0.8	2.3 ± 1.0
2nd Radiation oncologist	1.5 ± 0.5	3.5 ± 0.5	3.0 ± 1.0

The weighted Kappa for inter-observer reliability was analyzed by SPSS version 22. The result shows that it is not a significant difference in both radiation oncologists in interpretation in image scoring. The difference in efficiency between the new method and FBP was significant ($p < 0.05$), but not for OMAR ($p > 0.05$).

4.5 Discussion

The source of metal artifact in the oral cavity of computed tomographic images is metal filled in the teeth. It suppresses the diagnosis, misdiagnoses and organ delineation in computed tomographic images. The new method was created based on the B-spline and averagely weighted interpolation techniques. This study was analyzed in CT number according to equation 19 to convert the pixel to CT number in MATLAB software.

$$CT\ number = (Gray\ value\ \times Slope) + Intercept \quad ...20$$

This results on a homogeneous phantom and Alderson Rando phantom show that the metal artifact suppressed by the new method is better than filtered back projection and OMAR. In contrast, the clinical study indicated that OMAR is better than a new method and filtered back projection in the suppression of the metal artifact. The performance of the new method of metal artifact reduction depends on the number, size, and site of amalgam in the oral cavity and also depends on the image quality of the adjacent image. The percent of the success of the new method of metal artifact reduction in clinical data was 96.2% (50 from 52 images).

The Intel® Core™ 2 Quad CPU Q9300 @2.5 GHz, 4 GB memory with Window 7 32-bit for image processing had been used in this study. The processing time of the new algorithm was less than 1 minute because of the simple equation and effective method.

The acquisition parameter of CT was spiral scan mode, 120 kVp, 100 to 200 mAs, 16 x 1.5 mm collimation, 3 mm slice thickness, 0.938 pitch factor, 0.75 s rotation time, 512 x 512 matrix size in all CT images. The quality control procedures of Philips Brilliance Big Bore CT scanner are according to AAPM report No. 39, AAPM TG No 66 and IAEA human health series No. 19 before studied. The procedures are separated into three parts; radiation safety, mechanical and image quality.

The three-millimeter slice thickness was used in this study as in the routine clinical practice of Division of Radiation Oncology, Department of Radiology, King Chulalongkorn Memorial Hospital according to RTOG number 0615 protocol. If slice thickness of CT was increased, the metal artifact would be decreased. In contrast, if slice thickness of CT was decreased, the metal artifact would be increased, but the information of CT will be more than a thicker slice.

The B-spline parameter in this study was 3 for knot and 2 for the degree. However, this study also studied these parameters. This study indicated that the number of knot and degree of power of B-spline affect to the image quality of the corrected image. When increasing the number of a knot in B-spline, it also increases of a number of points in the B-spline method. The power of a degree in B-spline, If the power of degree is added, the resulting image does not meet the specified knot that describes before.

The α parameter of the averagely weighted equation for interslice interpolation was fixed to 0.5 in all CT images. However, this study also varied this parameter from 0.1 to 0.9. The result indicated that the image quality of the corrected image depends on the image quality of adjacent images. If higher α closed to the better image quality, the image quality of the corrected image was excellent.

The second averagely weighted equation (equation 19) used to merge the result from B-spline (intra-slice interpolation) and inter-slice interpolation. This study varied the α parameter and found that the image quality of the corrected CT image depends on image quality that used for the input parameter. The image quality of the input image is the primary factor that affects to the image quality of the corrected CT image in term of metal artifact reduction.

The quantitative evaluation was the percentage of noise which could represent the image quality in terms of the artifact. The pixel value has not been analyzed because it could not represent the image quality in terms of metal streak artifact. The pixel value does not represent the image quality in terms of metal streak artifact because most of the streak artifact is pronounced in bright area than dark area. When the bright area is large, the pixel value is too high compared to the standard deviation. This results in low percent noise, but more metal streak artifact in the CT images.

Several publications (3-6, 10-12, 19, 20, 23) reported the performance of metal artifact reduction method by sinogram technique and forward projection metal artifact reduction technique. Most of the new methods showed much better performance than filtered back projection method in qualitative and quantitative evaluations. Most publications studied in the phantom or simulation phase without the clinical applications. This study shows both phantom and clinical applications which the new method could reduce the metal artifact in phantom and patients. The performance of the new method shows better image quality than the filtered back projection method.

The new method of metal artifact reduction can be used in several CT scanner vendors because it uses the DICOM format in image processing.

4.6 Recommendation

There is an unexpected new artifact consequence where the new method may modify more artifacts. The radiologist and radiation oncologist should always compare filtered back projection and new method dataset in clinical applications

Chapter 5
Conclusion

The computed tomographic image is essential for diagnostic and therapeutic purposes in various medical disciplines. The common artifact in computed tomography is motion, ring and metal artifact. The methods to solve motion and ring artifact are available but the metal artifact still in development. The new metal artifact method in this study based on the B-spline and averagely weighted interpolation techniques. The new method could suppress the metal artifact of CT images in head and neck region and improve image quality and diagnostic confidence in the metallic artifact region.

The efficiency of the new method is better than filtered back projection and OMAR in homogeneous phantom and Alderson Rando phantom in clinical range of tube current time, mAs. However, the efficiency of the new method and MAR is comparable, and both methods are better than filtered back projection regarding percent noise. The image quality scoring by two independent radiation oncologists with the same experience shows comparable efficiency result of the new method and OMAR. The result showed the higher accuracy in interpretation of CT images according to both qualitative and quantitative analysis. The values of the new metal artifact method are simple, fast in image processing and available in several CT vendors because it is using the DICOM format in the image processing.

REFERENCES

1. Bushberg JT. The essential physics of medical imaging: Lippincott Williams & Wilkins; 2002.
2. Barrett JF, Keat N. Artifacts in CT: recognition and avoidance. Radiographics. 2004;24(6):1679-91.
3. Boas FE, Fleischmann D. Evaluation of two iterative techniques for reducing metal artifacts in computed tomography. Radiology. 2011;259(3):894-902.
4. De Man B, Nuyts J, Dupont P, Marchal G, Suetens P, editors. Metal streak artifacts in X-ray computed tomography: a simulation study. Nuclear Science Symposium, 1998 Conference Record 1998 IEEE; 1998: IEEE.
5. De Man B, Nuyts J, Dupont P, Marchal G, Suetens P. Reduction of metal streak artifacts in x-ray computed tomography using a transmission maximum a posteriori algorithm. IEEE transactions on nuclear science. 2000;47(3):977-81.
6. Lemmens C, Faul D, Nuyts J. Suppression of metal artifacts in CT using a reconstruction procedure that combines MAP and projection completion. IEEE transactions on medical imaging. 2009;28(2):250-60.
7. Popilock R, Sandrasagaren K, Harris L, Kaser KA. CT artifact recognition for the nuclear technologist. J Nucl Med Technol. 2008;36(2):79-81.
8. Hsieh J, Nett B, Yu Z, Sauer K, Thibault J-B, Bouman CA. Recent advances in CT image reconstruction. Current Radiology Reports. 2013;1(1):39-51.
9. Wang G, Snyder DL, O'Sullivan JA, Vannier MW. Iterative deblurring for CT metal artifact reduction. IEEE Trans Med Imaging. 1996;15(5):657-64.
10. Wang G, Vannier MW, Cheng PC. Iterative X-ray Cone-Beam Tomography for Metal Artifact Reduction and Local Region Reconstruction. Microsc Microanal. 1999;5(1):58-65.
11. Yu H, Zeng K, Bharkhada DK, Wang G, Madsen MT, Saba O, et al. A segmentation-based method for metal artifact reduction. Acad Radiol. 2007;14(4):495-504.

12. Roeske JC, Lund C, Pelizzari CA, Pan X, Mundt AJ. Reduction of computed tomography metal artifacts due to the Fletcher-Suit applicator in gynecology patients receiving intracavitary brachytherapy. Brachytherapy. 2003;2(4):207-14.

13. Healthcare P. Metal artifact reduction for orthopedic implants (O-MAR). White Paper, Jan. 2012.

14. Van Slambrouck K. Local models and local convergence for maximum likelihood iterative reconstruction. 2013.

15. Lecchi M, Fossati P, Elisei F, Orecchia R, Lucignani G. Current concepts on imaging in radiotherapy. European journal of nuclear medicine and molecular imaging. 2008;35(4):821-37.

16. Mouton A, Megherbi N, Van Slambrouck K, Nuyts J, Breckon TP. An experimental survey of metal artefact reduction in computed tomography. J Xray Sci Technol. 2013;21(2):193-226.

17. Kak A. M. Slaney M. Principle of Computerized Tomographic Imaging. 1998.

18. Lewis M, Reid K, Toms AP. Reducing the effects of metal artefact using high keV monoenergetic reconstruction of dual energy CT (DECT) in hip replacements. Skeletal radiology. 2013;42(2):275-82.

19. Joemai RM, de Bruin PW, Veldkamp WJ, Geleijns J. Metal artifact reduction for CT: development, implementation, and clinical comparison of a generic and a scanner-specific technique. Med Phys. 2012;39(2):1125-32.

20. Koehler T, Brendel B, Brown K, editors. A New Method for Metal Artifact Reduction. The Second International Conference on Image Formation in X-ray Computed Tomography, June 24-27, 2012, Salt Lake City, Utah, USA; authors version; 2012.

21. Li H, Noel C, Chen H, Harold Li H, Low D, Moore K, et al. Clinical evaluation of a commercial orthopedic metal artifact reduction tool for CT simulations in radiation therapy. Med Phys. 2012;39(12):7507-17.

22. Sornjarod Oonsiri PK, Mana Sriyudthasak, Anchali Krisanachinda, Sivalee Suriyapee, David Sutton, editor Implementation of OMAR in treatment planning system. 14th Asia-Oceania Congress of Medical Physics and 12th South East Asia

Congress of Medical Physics; 2014 23-25 October 2014; Ho Chi Minh City, Vietnam2014.

23. Giantsoudi D, De Man B, Verburg J, Trofimov A, Jin Y, Wang G, et al. Metal artifacts in computed tomography for radiation therapy planning: dosimetric effects and impact of metal artifact reduction. Physics in Medicine & Biology. 2017;62(8):R49.

24. Wagenaar D, van der Graaf ER, van der Schaaf A, Greuter MJ. Quantitative comparison of commercial and non-commercial metal artifact reduction techniques in computed tomography. PLoS One. 2015;10(6):e0127932.

25. Anderla A, Culibrk D, Delso G, Mirkovic M. MR image based approach for metal artifact reduction in X-ray CT. ScientificWorldJournal. 2013;2013:524243.

26. Park PC, Schreibmann E, Roper J, Elder E, Crocker I, Fox T, et al. MRI-based computed tomography metal artifact correction method for improving proton range calculation accuracy. Int J Radiat Oncol Biol Phys. 2015;91(4):849-56.

27. Gonzalez RC, Woods RE. Digital image processing. Upper Saddle River, NJ: Prentice Hall; 2012.

28. Piegl L, Tiller W. The NURBS Book 2nd edition. 1997.

29. Unser MA, editor Splines: a perfect fit for medical imaging. Medical Imaging 2002: Image Processing; 2002: International Society for Optics and Photonics.

APPENDIX

Quality control of computed tomography

Equipment: PHILIPS

Model: Brilliance CT Big Bore **Serial number:** 7939

Max kVp: 140 **Max mA:** 500

Phantom: Catphan phantom 412

Result

Test	Parameter	Suggested performance criteria	Actual results
CT number of water	Center	± 5	-0.1 SD 3.6
	0 degree	± 5	-2.1 SD 3.5
	90 degree	± 5	-1.7 SD 3.4
	180 degree	± 5	-1.3 SD 3.2
	270 degree	± 5	-1.6 SD 3.3
Accuracy of distance measurement		≤ 1 mm	0.03 mm
Table incrementation		≤ 3 mm	0.1 mm
Noise		± 15%	0.33%
Slice thickness	1.5 mm	0.75 mm	1.58 mm
	3.0 mm	1.00 mm	3.02 mm
	6.0 mm	1.00 mm	6.02 mm
	9.0 mm	1.00 mm	8.97 mm
Linearity	Air	-1000	-982.1 SD 110.4
	LDPE	-90	-116.7 SD 23.4
	Delrin	370	361.2 SD 42.2
	Teflon	990	977.7 SD 137.6
	Linear correlation coefficient	> 0.99	0.9995
High contrast resolution		≥ 5 lp/cm	7 lp/cm
Low contrast resolution		≤ 5 mm at 0.5%	3 mm at 0.5%
Uniformity		± 4 HU from center	3.5 HU from center

Radiation survey

Parameter **kVp:** 120 **mAs:** 350 **Rotation time:** 0.75 s

Scan time: 10.70 s **Slice thickness:** 3 mm

Equipment: Fluke survey meter **Model:** 451P-DE-SI-RYP **Serial number:** 6608

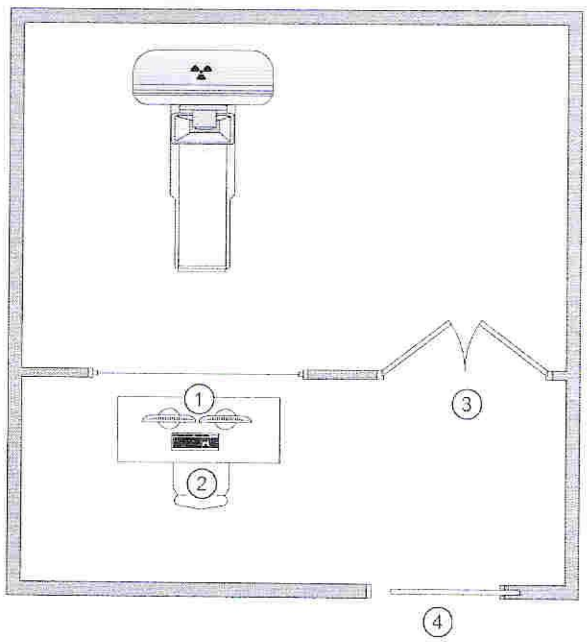

Location	Dose (μSv/hr)	Dose limit (μSv/hr)
1. Behind lead glass	1	2
2. Control	< 1	1
3. Door (Close)	2	4
4. Door (Open)	< 1	< 1

VITA

Name	Sornjarod Oonsiri
Gender	Male
Nationality	Thai
Date of birth	2 March 1981
Place of birth	Bangkok, Thailand
Year of graduation	Mahidol University, 2003
	Bachelor of Science (Radiological Technology)
	Chulalongkorn University, 2005
	Master of Science (Medical Imaging)
	Chulalongkorn University, 2018
	Doctor of Philosophy (Biomedical Engineering)
Home address	41 Soi Inthamara 8, Suthisarn-vinitchai road
	Phayathai, Bangkok, Thailand 10400